NAVAL POSTGRADUATE SCHOOL

Monterey, California

THESIS

Natural Convection Liquid Immersion Cooling
of a Column of Discrete Heat Sources
in a Vertical Channel

by

Daniel L. Knight

September 1988

Thesis Advisor: Yogendra Joshi

Approved for public release; distribution is unlimited

UNCLASSIFIED

SECURITY CLASSIFICATION OF THIS PAGE

REPORT DOCUMENTATION PAGE

1a. REPORT SECURITY CLASSIFICATION UNCLASSIFIED	1b RESTRICTIVE MARKINGS
2a. SECURITY CLASSIFICATION AUTHORITY	3 DISTRIBUTION / AVAILABILITY OF REPORT Approved for public release; distribution is unlimited
2b. DECLASSIFICATION / DOWNGRADING SCHEDULE	
4 PERFORMING ORGANIZATION REPORT NUMBER(S)	5 MONITORING ORGANIZATION REPORT NUMBER(S)
6a. NAME OF PERFORMING ORGANIZATION Naval Postgraduate School 6b OFFICE SYMBOL (If applicable) 69	7a NAME OF MONITORING ORGANIZATION
6c. ADDRESS (City, State, and ZIP Code) Monterey, California 93943-5000	7b. ADDRESS (City, State, and ZIP Code) Monterey, California 93943-5000
8a. NAME OF FUNDING / SPONSORING ORGANIZATION 8b OFFICE SYMBOL (If applicable)	9. PROCUREMENT INSTRUMENT IDENTIFICATION NUMBER
8c. ADDRESS (City, State, and ZIP Code)	10 SOURCE OF FUNDING NUMBERS PROGRAM ELEMENT NO. / PROJECT NO. / TASK NO / WORK UNIT ACCESSION NO.

11. TITLE (Include Security Classification)
Natural Convection Liquid Immersion Cooling of a Column of Discrete Heat Sources in a Vertical Channel

12. PERSONAL AUTHOR(S)
KNIGHT, Daniel L.

13a. TYPE OF REPORT	13b TIME COVERED	14. DATE OF REPORT (Year, Month, Day)	15 PAGE COUNT
Master's Thesis	FROM _____ TO _____	1988 September	63

16 SUPPLEMENTARY NOTATION
The view expressed in this thesis are those of the author and do not reflect the official policy or position of the Department of Defense or the US Government

17 COSATI CODES			18. SUBJECT TERMS (Continue on reverse if necessary and identify by block number)
FIELD	GROUP	SUB-GROUP	Convective Flow, Thermal Transport, Flow Visualization, Theses, Cjkd / c

19. ABSTRACT (Continue on reverse if necessary and identify by block number)

Natural convection from a single column of eight in-line, rectangular, flush heat sources was examined. A vertical channel was formed by placing a movable shroud parallel to the test surface. The experimental program consisted of temperature measurements and flow visualizations. For a range of component power levels and channel spacings, surface temperatures of each heat source were measured at five locations using embedded thermocouples The resulting steady state data was compared with corresponding measurements for an identical geometric arrangement of protruding heat sources. The flow visualization was carried out using a laser generated plane of light. Keywords:

20. DISTRIBUTION / AVAILABILITY OF ABSTRACT	21. ABSTRACT SECURITY CLASSIFICATION
☒ UNCLASSIFIED/UNLIMITED ☐ SAME AS RPT. ☐ DTIC USERS	UNCLASSIFIED
22a. NAME OF RESPONSIBLE INDIVIDUAL Prof Joshi	22b. TELEPHONE (Include Area Code) (408)646-3400 / 22c OFFICE SYMBOL 69Ji

DD FORM 1473, 84 MAR 83 APR edition may be used until exhausted. All other editions are obsolete

SECURITY CLASSIFICATION OF THIS PAGE

UNCLASSIFIED

Approved for public release; distribution is unlimited

Natural Convection Liquid Immersion Cooling of a Column of Discrete Heat Sources in a Vertical Channel

by

Daniel L. Knight
Lieutenant, United States Navy
B.S., The Citadel, 1979

Submitted in partial fulfillment of the
requirements for the degree of

MASTER OF SCIENCE
IN MECHANICAL ENGINEERING

from the

NAVAL POSTGRADUATE SCHOOL

September 1988

Author: 
Daniel L. Knight

Approved by: 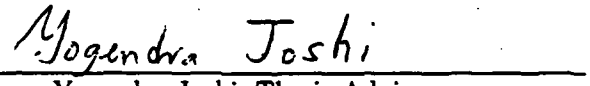
Yogendra Joshi, Thesis Advisor

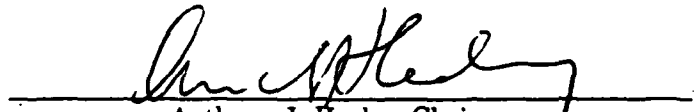
Anthony J. Healey, Chairman
Department of Mechanical Engineering


Gordon E. Schacher
Dean of Science and Engineering

ABSTRACT

Natural convection from a single column of eight in-line, rectangular, flush heat sources was examined. A vertical channel was formed by placing a movable shroud parallel to the test surface. The experimental program consisted of temperature measurements and flow visualizations. For a range of component power levels and channel spacings, surface temperatures of each heat source were measured at five locations using embedded thermocouples. The resulting steady state data was compared with corresponding measurements for an identical geometric arrangement of protruding heat sources. The flow visualization was carried out using a laser generated plane of light.

TABLE OF CONTENTS

LIST OF FIGURES

LIST OF SYMBOLS

Symbol	Description	Units
A	Area	m^2
A_s	Heater Surface Area	m^2
g	Acceleration due to Gravity	$\frac{m}{s^2}$
Gr^*	Flux-based Grashof Number	Dimensionless
h	Heat Transfer Coefficient	$\frac{W}{m^2K}$
k_f	Fluid Thermal Conductivity	$\frac{W}{mK}$
k_{pg}	Plexiglass Thermal Conductivity	$\frac{W}{mK}$
L	Test Surface Length	m
$\bar{L}$	Characteristic Length	m
Nu	Nusselt Number	Dimensionless
Nu^*	Modified Nusselt Number	Dimensionless
NDT	Non-dimensional Temperature Excess	Dimensionless
P	Prandtl Number	Dimensionless
q''	Energy Flux Convected into the Fluid per Component	$\frac{W}{m^2}$
Q_{COND}	Energy Loss via Conduction Through the Test Surface	W
Q_{CONV}	Energy Convected into the Fluid per Component	W
Q_{in}	Energy into each Heater	W
S_n	Heater Element Number in Relation to the Leading Component	Dimensionless

T	Local Surface Temperature	$°C$
T_{amb}	Ambient Temperature	$°C$
T_{avg}	Average Component Temperature	$°C$
T_{film}	Film Temperature at which Fluid Properties are Evaluated	K
T_s	Surface Temperature	$°C$
v	Specific Volume	$\frac{m^3}{kg}$
x	Vertical Distance from Bottom Edge of Test Surface	m
z	Horizontal Distance from Component Center	m
β	Expansion Coefficient	$\frac{1}{K}$
μ	Dynamic Viscosity	$\frac{N_s}{m^2}$
ν	Kinematic Viscosity	$\frac{m^2}{s}$
θ	Temperature Difference Between Local Temperature and Ambient	K
θ_o	Temperature Scaling Factor	K

ACKNOWLEDGMENT

Natural convection from a single column of eight in-line, rectangular, flush heat sources was examined. A vertical channel was formed by placing a movable shroud parallel to the test surface. The experimental program consisted of temperature measurements and flow visualizations. For a range of component power levels and channel spacings, surface temperatures of each heat source were measured at five locations using embedded thermocouples. The resulting steady state data was compared with corresponding measurements for an identical geometric arrangement of protruding heat sources. The flow visualization was carried out using a laser generated plane of light.

I. INTRODUCTION

A. STATEMENT OF PROBLEM

With each successive increase in the scale of integration of micro-electronic circuits, there has been a need to improve cooling technologies. Currently, chip heat fluxes are approaching 50 W/cm^2, [Ref. 1]. Heat dissipation may be improved by using higher velocities of air, chilled water heat exchangers, or altering the system design to reduce its thermal resistance. These techniques are becoming less satisfactory and the limits of air and indirect liquid cooling have nearly been reached. If projected heat fluxes of 200 W/cm^2, [Ref. 1], are to be achieved, then direct liquid immersion becomes an attractive option, [Ref. 1, 6].

The performance and reliability of micro-electronic devices are very sensitive to junction temperatures. The failure rate of chips increase exponentially as the junction temperature increases. The long term reliability of circuit chips can be improved by 50% with every $10°C$ decrease in temperature that the device is maintained below its maximum operating temperature, [Ref. 2, 3, 4].

For a complete thermal analysis of any electronic package design, all three modes of heat transfer must be considered. Radiation effects are significant primarily in systems involving air cooling. Effects of conduction, however, must be evaluated in each cooling application. These may also be substantial during transients.

The convection heat transfer rate from a surface at temperature T_s with exposed surface area A to its surrounding fluid at temperature T_{amb} is given by Newton's Law of Cooling:

$$q = hA(T_s - T_{amb}) \tag{1.1}$$

This is the definition of h, the convective heat transfer coefficient and not a phenomenological law.

Most available correlations for the convective heat transfer coefficient are usually valid for large heat sources. These are often good for determining the overall heat transfer from a single circuit board. Individual devices mounted on the substrate act as discrete heat sources and typically have higher average temperatures than those predicted by such text book correlations [Ref. 6].

Convection may be either forced or natural. Forced convection relies on a prime mover to displace the fluid and cause it to flow over the electronic package. This method of convection yields very high heat transfer coefficients and may become one of the primary means of cooling electronic packages as component heat fluxes continue to rise. Natural convection or buoyancy induced flow, results from body forces acting on density differences within the fluid. In many applications, these density gradients result due to the presence of temperature variations. The heat transfer coefficients are smaller than those associated with forced convection since the flow velocities are generally much smaller for natural convection. However, the resulting design of the package can be considerably simpler and more reliable than in other cooling arrangements.

B. OBJECTIVES

This experimental study was undertaken to determine the hydrodynamic and thermal characteristics of buoyancy induced flow resulting from several flush mounted

discrete heat sources on a vertical surface. The results from this study will be compared to those in Reference 7 where an array of rectangular protruding heat sources was used.

A single column of discrete heat sources was chosen since it provided a simple geometric arrangement simulating some of the modern electronic packages such as flat packs.

Specific objectives of this study were:

- To visualize the steady-state natural convection flow within a channel over a range of component power levels and channel widths.
- To measure component temperatures at each power level and channel width and develop heat transfer relationships for this geometry.
- To measure the temperature distribution within the fluid adjacent to the heated surface in the absence of a shrouding wall.

This study advances the work described in References 5 and 7 and is part of an ongoing effort to study natural convection liquid immersion cooling of electronic equipment.

II. EXPERIMENTAL

A. GENERAL DESIGN CONSIDERATION

Equipment design and construction details are provided in Reference 5. Only system changes and a brief overview is presented here.

As seen in Figure 2.1, the test assembly consists of eight flush mounted foil heaters. Each heater (Figure 2.2) is a network of Inconel 600 conductor mounted on a Kapton backing. The heaters measured 23.9 mm in width by 7.8 mm in height. They formed a single column on a plexiglass substrate. The substrate measured 25.4 mm square and was 12.7 mm thick. The column of heaters was centered on the substrate and each heater was spaced 25.4 mm center to center from an adjacent heater. Another piece of plexiglass identical to the substrate without the heaters was used as an adjustable shroud wall to form the channel. This shroud was used to simulate the back side of a neighboring circuit board.

Five copper-constantan thermocouples of 0.127 mm diameter wire were used for temperature measurements on each heater. The thermocouples were embedded within 6 mm deep slots in the substrate. For each heater, one thermocouple bead was located at the foil center and the remaining four were at the centers of each edge of the heater. All wires were routed along 6 mm deep grooves cut below the heater placement slots. All wiring came out through the back of the test surface through drilled holes in the substrate. After all heaters and wires were in place, these holes were sealed with a low conductivity adhesive. Omega Bond 101, a high conductivity adhesive, was used to bond the thermocouples in place and to electrically insulate the thermocouple beads from the heater foils. A sixth thermocouple for each heater

Figure 2.1: Assembled Test Surface

was centered behind the heater on the back side of the plexiglass substrate. This was used to estimate conduction losses through the substrate.

A 0.127 mm diameter, copper-constantan thermocouple probe (Figure 2.3) was constructed. This probe was attached to a three dimensional traverse and used to measure the temperature distribution within the fluid adjacent to the test surface. The foil heaters were powered using a regulated D.C. power supply as described in Reference 5.

The test surface was immersed in an open, one cubic meter tank constructed from plate glass and insulated on all sides. For flow visualization, particles of pliolite were suspended in the de-ionized water. Pliolite is an inert substance with a specific gravity of 0.93. These particles were illuminated by aiming an eight milliwatt helium neon laser through a cylindrical lens to split the light beam into a plane of light.

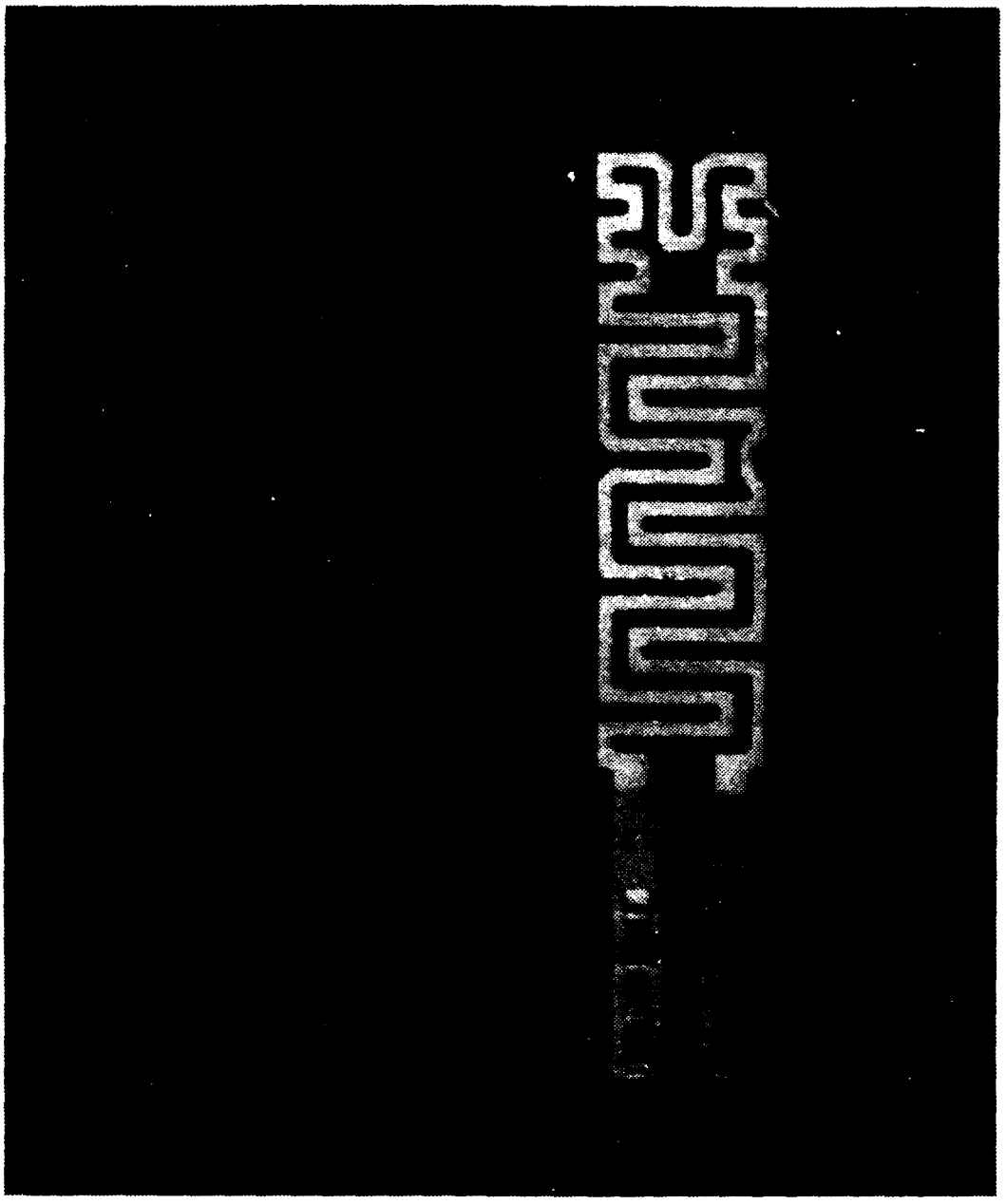

Figure 2.2: Foil Heater

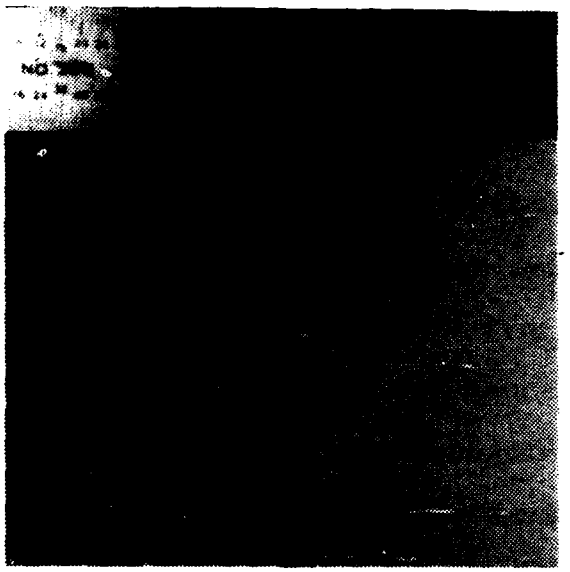

Figure 2.3: Traversing Thermocouple Probe

By using a motor driven camera and an intervalometer, extended time exposure photographs of the flow patterns within the illuminated plane were obtained.

B. EXPERIMENTAL PROCEDURE

Details of data acquisition techniques are provided in Reference 5, hereafter referred to as the initial study. The follow-on study by Willson [Reference 7] will be referred to as the previous study.

Power settings of 0.2, 0.5, 1.0, 1.2, 1.5, and 2.0 watts were used for each channel width. The shroud was adjusted for channel spacings of 1.5 mm, 3.0 mm, 5.0 mm, 9.0 mm, 12.0 mm and 15.0 mm. With the shroud removed, an infinite channel spacing was created.

When measuring the steady state temperatures of each heater element, measurements were taken at 10 minute intervals and compared with the previous data

run. When all thermocouple measurements varied less than $0.05°C$, the final steady state temperature measurements were recorded. The termperature acquisition program of the previous study [Appendix A] was executed to record and store data.

Ambient temperature was the average temperature from three thermocouples located in the fluid near the top, bottom and center of the tank. All experiments were stopped if these three temperatures varied by more than $0.1°C$.

When measuring the fluid temperature with the movable probe, the data acquisition computer was programmed to continuously monitor the voltage output from the traversing thermocouple probe. This allowed for point to point temperature measurements within the flow.

After all data was recorded, the substrate was painted black to minimize light reflection. Particles of pliolite were mixed with the distilled water to visualize fluid flow. The f stop of the camera was set to 2.8 and exposure time for all photographs was 20 seconds. The camera was mounted on a tripod, approximately three inches from the glassplate wall of the tank. Camera height was adjusted and the laser was aligned so that all eight heater surfaces would be in the field of view. When the shroud was in position, the camera angle was inclined slightly to avoid the undesirable light reflection off the shroud. A shroud spacing of 12 mm from the substrate was the minimum channel width at which useful pictures could be taken. Figure 2.4 shows the arrangement of the camera, laser and test surface.

C. DATA ANALYSIS

The convected rate of energy from each heater was determined using an energy balance where:

$$Q_{CONV} = Q_{in} - Q_{COND} \tag{2.1}$$

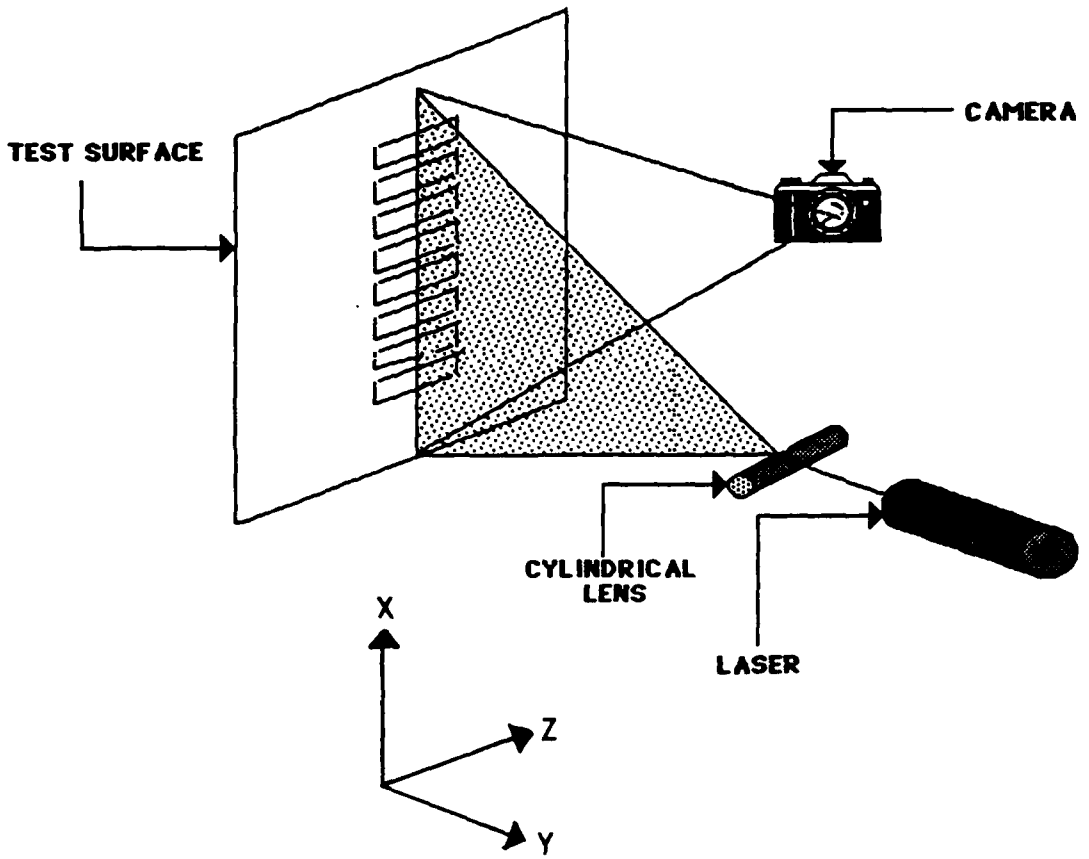

Figure 2.4: Laser and Camera Arrangement for Photography in the x-y Plane.

The energy in Q_{in} was regulated by the power supply and determined as described in the initial study. The energy loss by conduction was estimated by using Fourier's law of conduction for one dimension:

$$Q_{COND} = A_s k_{pg} \frac{\Delta T_{avg}}{\Delta x} \tag{2.2}$$

A_s is the surface area of each heater element, k_{pg} is the thermal conductivity for plexiglass. ΔT_{avg} is the temperature difference between the temperature average of the five thermocouple locations on the heater and the temperature at the back side of the substrate. Δx represents the minimum thickness of the substrate accounting for the grooves cut for wire routing.

A characteristic length, $\bar{L}$, based on the geometric dimensions of the heaters was chosen for determining non-dimensional temperature excess, $\frac{\theta}{\theta_o}$, a flux based Grashof number, Gr^*, and Nusselt number, Nu.

The characteristic length is the heater surface area divided by the heater perimeter.

$$\bar{L} = \frac{A_s}{p} \tag{2.3}$$

Local heat transfer relationships were determined by the following equations:

$$q'' = \frac{Q_{CONV}}{A_s} \tag{2.4}$$

$$\theta_o = \frac{q''\bar{L}}{k_f} \tag{2.5}$$

$$h = \frac{q''}{\Delta T} \tag{2.6}$$

$$Gr^* = \frac{g\beta q'' \bar{L}^4}{k_f \nu^2} \tag{2.7}$$

$$Nu = \frac{h\bar{L}}{k_f} \tag{2.8}$$

$$\theta = \Delta T \tag{2.9}$$

$$NDT = \frac{\theta}{\theta_o} \tag{2.10}$$

The data reduction program [Appendix A] was used for all calculations. Sample calculations are contained in Appendix B. The various symbols used above are defined in the List of Symbols.

Fluid properties were determined from curve fits listed by Willson [Reference 7]. These are based on the data provided in Incropera and Dewitt [Reference 8]. All properties were evaluated at a film temperature. The film temperature was determined for each case from the local and ambient temperatures.

A non-dimensional length, $\frac{X}{L}$, was used in the presentation of the data. The vertical length $\frac{X}{L}$ is the distance from the bottom edge of the substrate to the local point of interest divided by the overall length of the substrate.

Quantitive developments were expressed as plots of:

- Nu *vs.* Gr^*
- Non-dimensional local temperature excess vs. local thermocouple location.
- Temperature distribution in the fluid adjacent to the test surface.

III. TRANSPORT ADJACENT TO AN ISOLATED VERTICAL SURFACE

A. FLOW VISUALIZATION

Photographs of the steady state natural convection flow in the x-y plane are shown in Figure 3.1. The laser was aligned so that the plane of light would pass through the geometric center of the heated region of each component. This figure presents all elements at input power levels of 0.2, 1.0 and 2.0 watts respectively from left to right.

Buoyancy forces near the heaters create a strong upward flow. The flow appears to be laminar and is parallel to the substrate after the first component. A boundary layer begins to develop out from the leading heater. The boundary layer thickness increases to about 2.5 component heights at the trailing element. At 1.0 watt, the boundary layer is about 2.0 component heights thick and decreases to about 1.0 component height in thickness at the trailing element for 2.0 watts. The fluid velocity increases and the thickness of the boundary layer decreases with increasing component power input. Ambient fluid is entrained below and along the length of the boundary layer. Figure 3.2 visualizes the flow in the x-z plane at the respective power levels of the previous figure. The flow is vertical along the array for about the width of the heated region of the strips. Weak entrainment from the sides is evident. Side entrainment increases with increasing component heat input. Figure 3.2 clearly shows that for the region along the array, the flow can be treated to an excellent approximation as two dimensional.

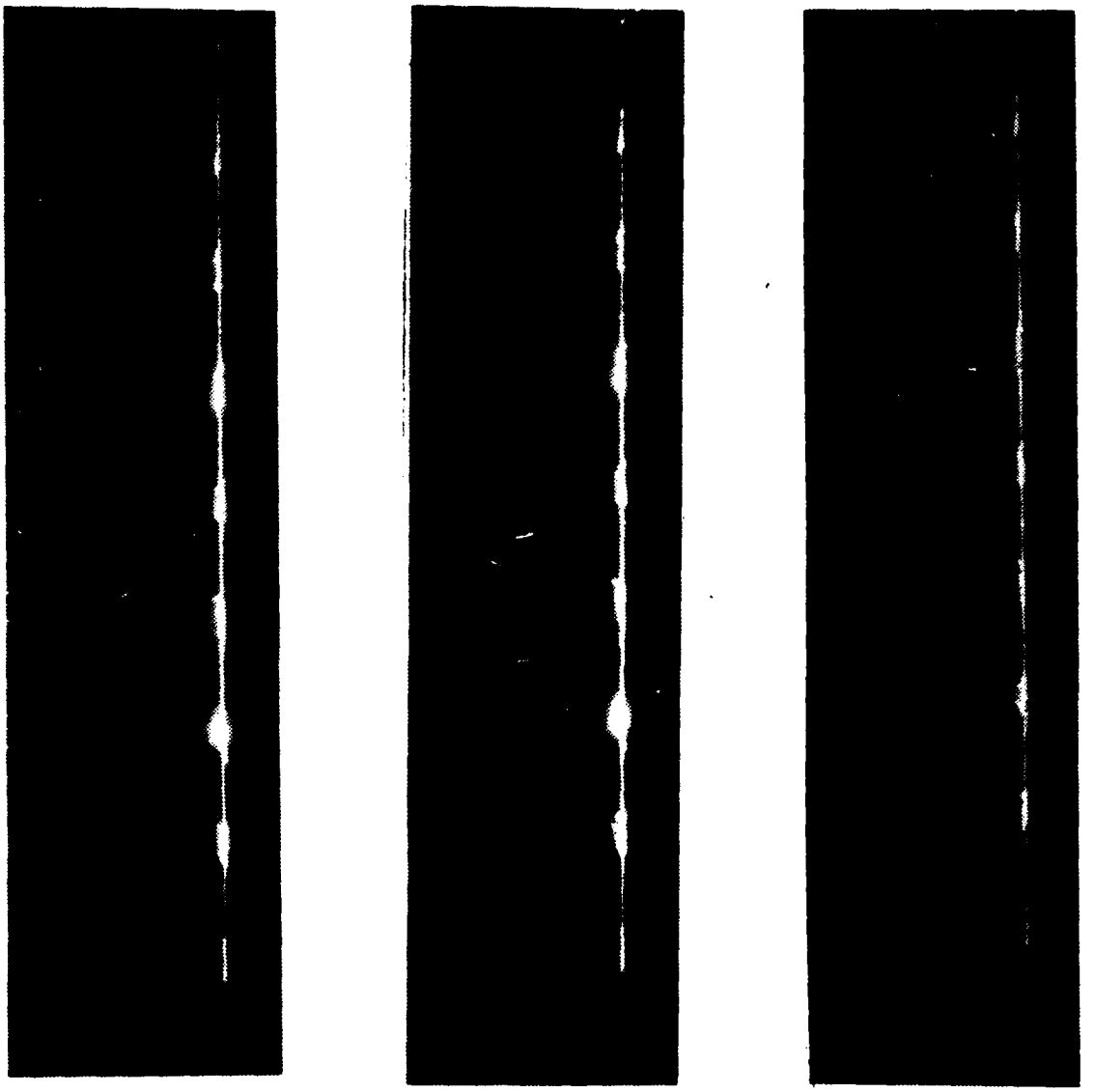

Figure 3.1: Steady Flow in the x-y Plane for Power Levels of 0.2, 1.0 and 2.0 Watts

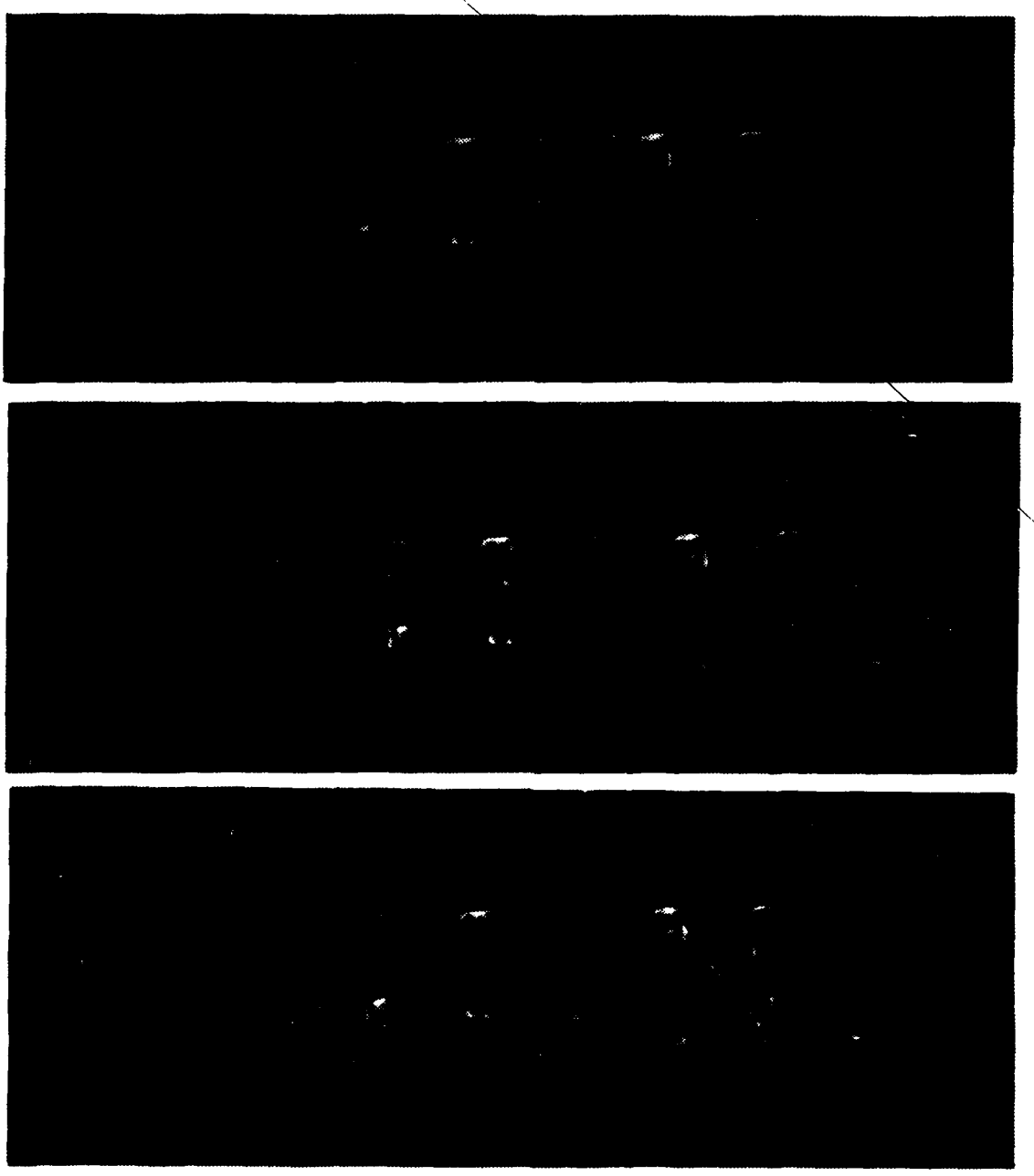

Figure 3.2: Flow in the x-z Plane at 0.2, 1.0 and 2.0 Watts

B. QUANTITATIVE

Figure 3.3 is a non-dimensional representation of local temperature excess levels measured at all thermocouple locations for an input power level of 2.0 watts. As expected, the measured component center temperatures were the highest. The top edge temperatures always exceeded the temperatures at the other edges. The left and right edge temperatures differed by a maximum of 22% at 2.0 watts. The heater strip had an 11 mm tab on the left side for power lead connections. Left edge conduction losses were therefore expected to be greater than the right side, resulting in slightly lower temperatures on the left. After the third component, the bottom edge temperatures exceeded the excess temperature of the sides. The side edges benefited more from fluid entrainment than the bottoms which are in the wake of the heated upstream components. In all experiments, the right edge temperature for component seven was lower than the established trend. It is believed that the thermocouple placement at this location may have slipped when the heater foil was pressed into place.

Heat transfer coefficients were computed from the data as outlined in equation 2.6. They indicated a downstream decreasing trend at a given power level. This is expected since the non-dimensional temperature excess is inversely proportional to h. As seen in Figure 3.3, the general trend tends to be increasing downstream excess temperatures.

As the component heat flux is increased, the buoyant flow becomes more vigorous. The component temperature levels, as a result, decrease. The calculated heat transfer coefficients are greater than those for the same component at lower power levels. With the larger values of h at higher power levels, there is a corresponding decrease in the non-dimensional temperature excess.

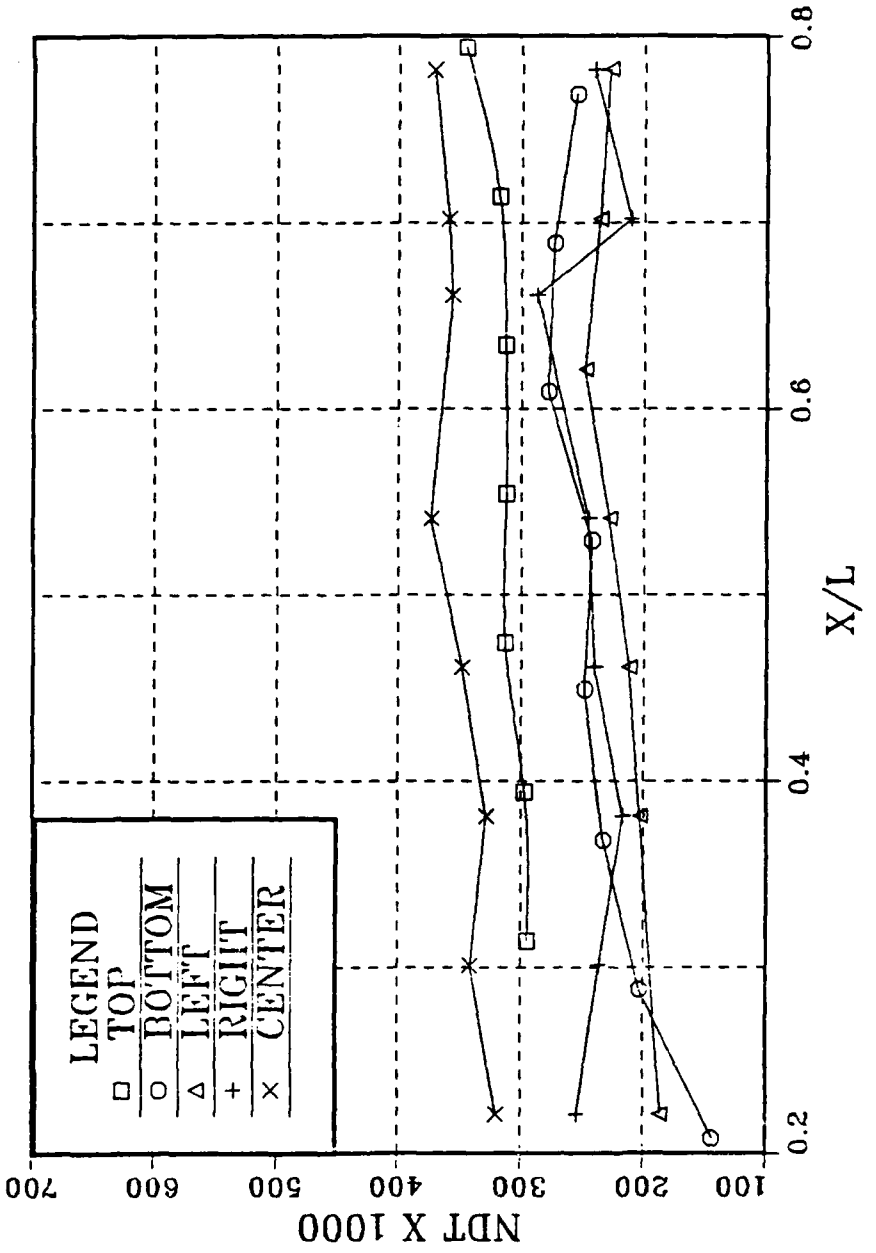

Figure 3.3: Non-dimensional Temperature Excess vs. Position: 2.0 Watts

Figure 3.4 is a logarithmic scatter plot of Nu vs. Gr^*. The cluster of data points at approximately a single Gr^* represents the Nusselt numbers for component centers at each power level. The Nusselt numbers decrease for downstream components, due to the increasing component temperatures.

As in the previous study, a modified Nusselt number, Nu^*, was calculated by using a scaling factor to account for the increase in convected energy of the flow at downstream locations.

$$Nu^* = Nu_n \times S_n^{\frac{1}{14}} \tag{3.1}$$

Nu_n and S_n are the local Nusselt numbers with the respective heater element numbers.

This modified data is plotted in Figure 3.5. The linear least squares fit through the data with a $\pm 5\%$ band is also presented. Using the scaling factor above, nearly all of the modified data falls within this band. Based on this curve fit, the following heat transfer relationship for the given array geometry was obtained:

$$Nu^* = 1.115(Gr^*)^{.12} \tag{3.2}$$

for $250 < Gr^* < 7000$ and $Pr \sim 7$.

C. EFFECT OF COMPONENT SPACING ON HEAT TRANSFER

Now that a heat transfer correlation has been developed for the given geometry of the array, it is desired to see how a change in component spacing would affect these relationships. This was achieved by powering every other and every third heater. This had the same effect as heater elements spaced 50.8 mm and 76.2 mm center to center. The resulting variations of non-dimensional temperature excess at the heater centers are shown in Figures 3.6 and 3.7.

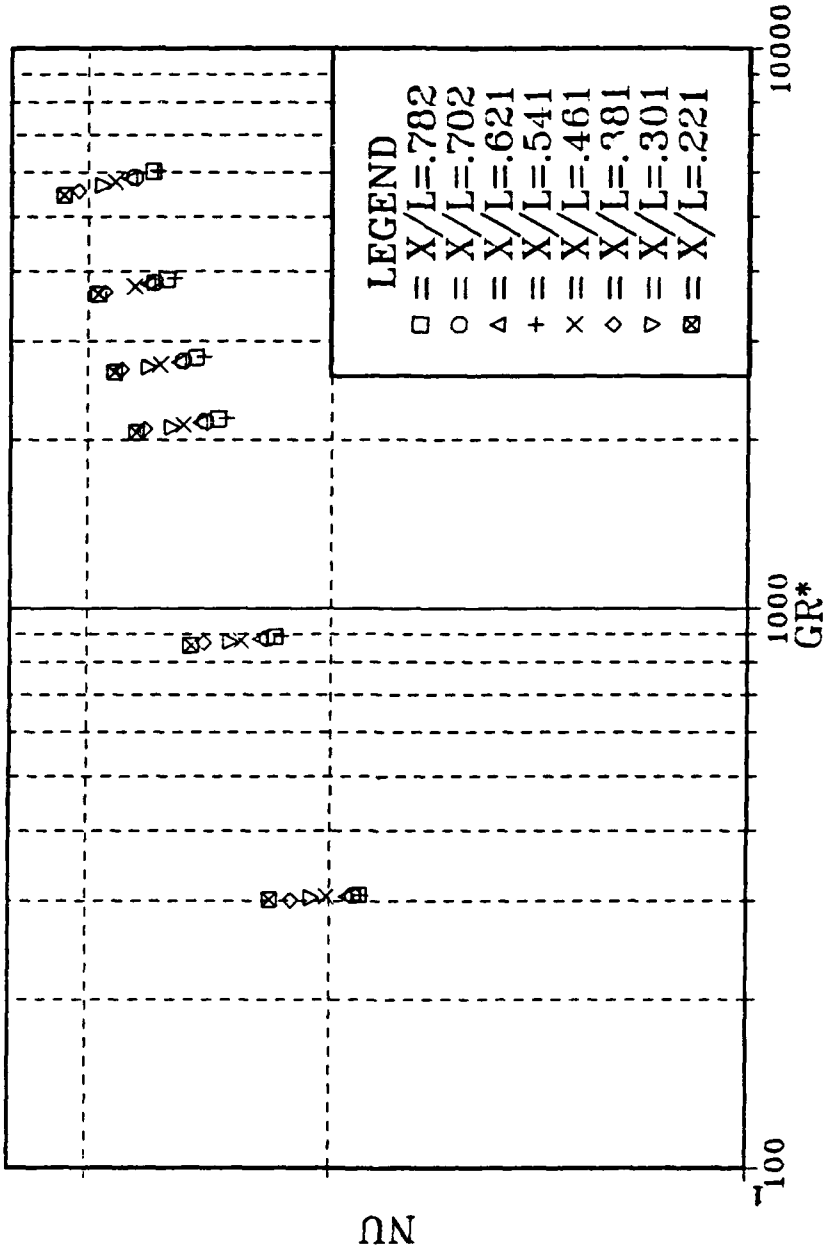

Figure 3.4: Data for Nusselt Number vs. Flux-Based Grashof Number

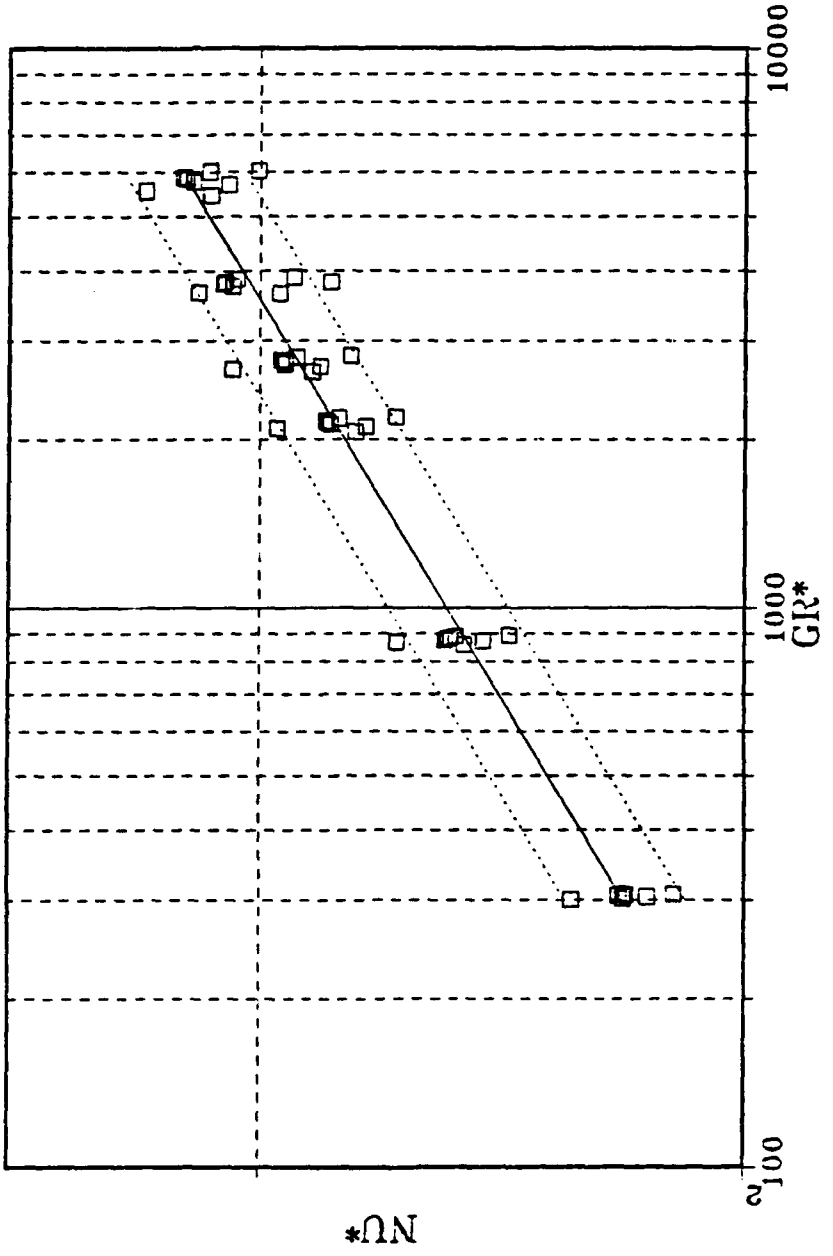

Figure 3.5: Modified Nusselt Number vs. Flux-Based Grashof Number with Least Squares Fit

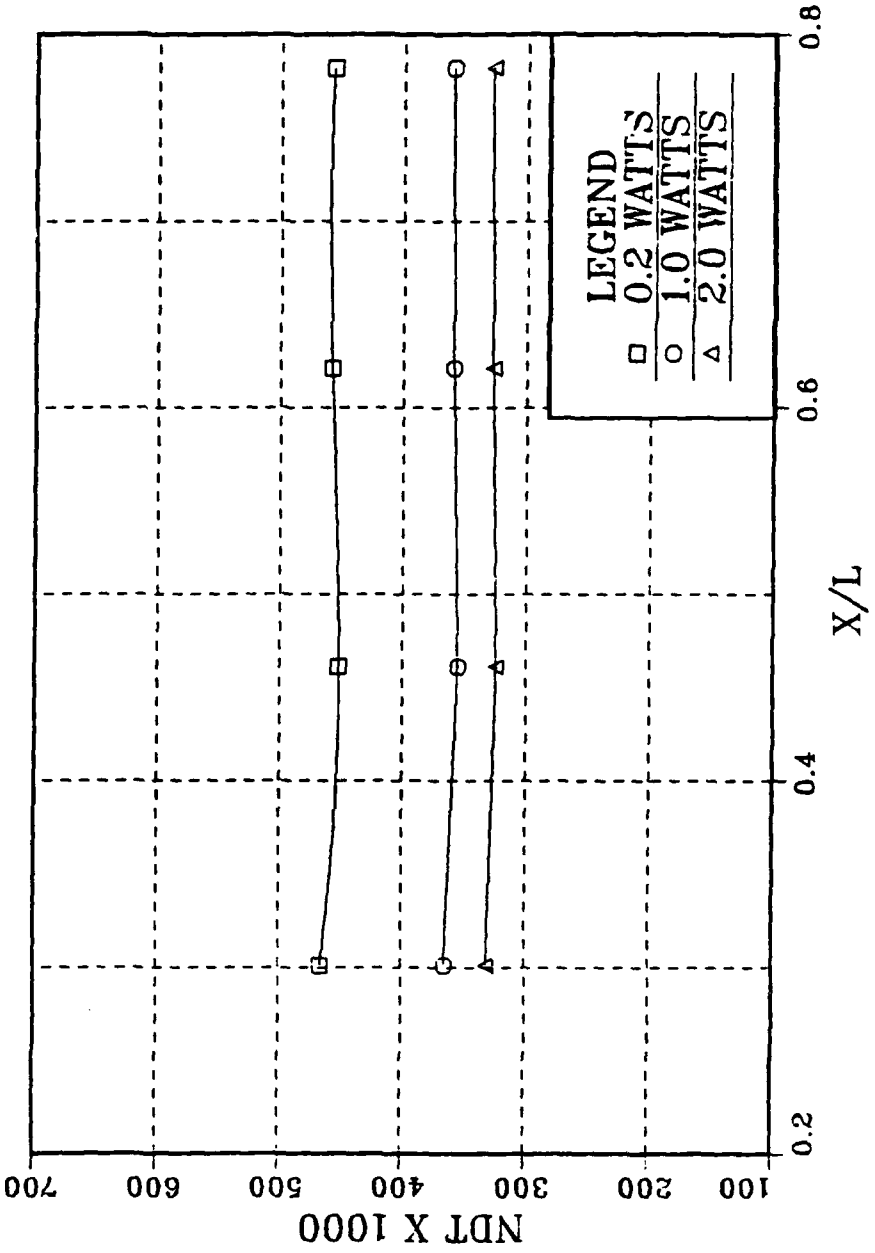

Figure 3.6: Non-dimensional Temperature Excess vs. Position with Four Elements Powered

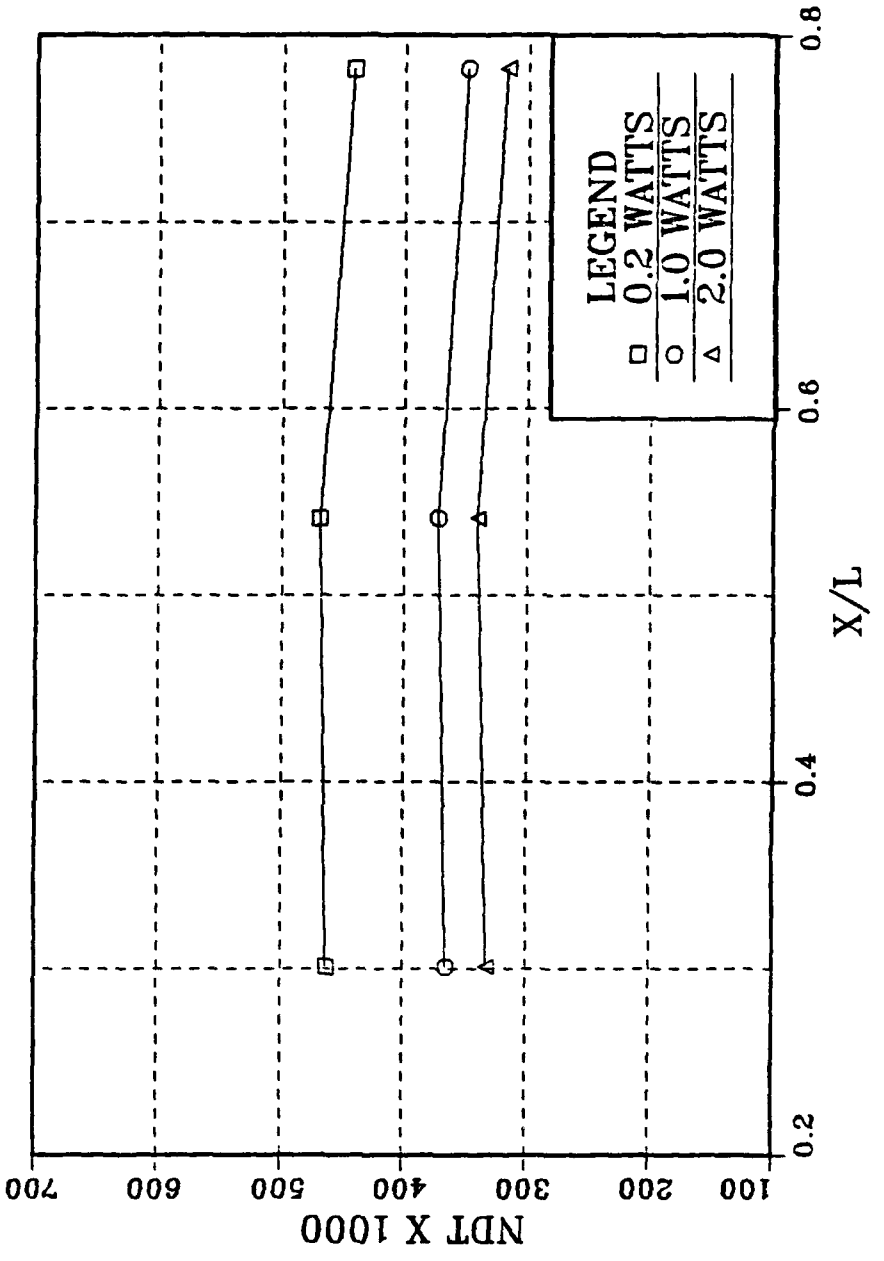

Figure 3.7: Non-dimensional Temperature Excess vs. Position with Three Elements Powered

When heaters 2, 4, 6 and 8 are powered, there is a slight decrease in the non-dimensional temperature at the first downstream component beyond the leading heater. Further up, component temperatures vary little from that of the second heater. When heaters 2, 5, and 8 are powered, the first two component temperatures remain unchanged. The trailing heater has a small drop in its non-dimensional temperature.

For the increased component spacings in Figures 3.6 and 3.7, the convected energy due to upstream heaters has only a weak effect on downstream components. The fluid momentum resulting from the buoyancy forces actually provides moderate improvement in heat transfer for the downstream heaters. Heat transfer relationships were obtained for all components by treating the elements in the array as single heaters. The resulting component based Nusselt numbers became almost independent of the downstream component position in the expanded array. These are plotted against the flux-based Grashof number in Figures 3.8 and 3.9. The least square fit to the correlated data for all unshrouded heaters is shown for comparison in each figure.

D. TEMPERATURE MEASUREMENTS WITHIN THE FLUID

Measurements of the thermal transport in the fluid adjacent to the test surface were made using the movable thermocouple probe. The thermocouple junction was initially centered on each component and then moved outward in the direction normal to the substrate. Temperatures are seen in Figure 3.10 for input power levels of 0.2 and 1.0 watts. The thermal boundary layer in both cases is well within the momentum exchange region which is approximately 1.6 cm thick for component 8 at 1.0 watt. This is expected due to the relatively large Pr of about 7.0 for water.

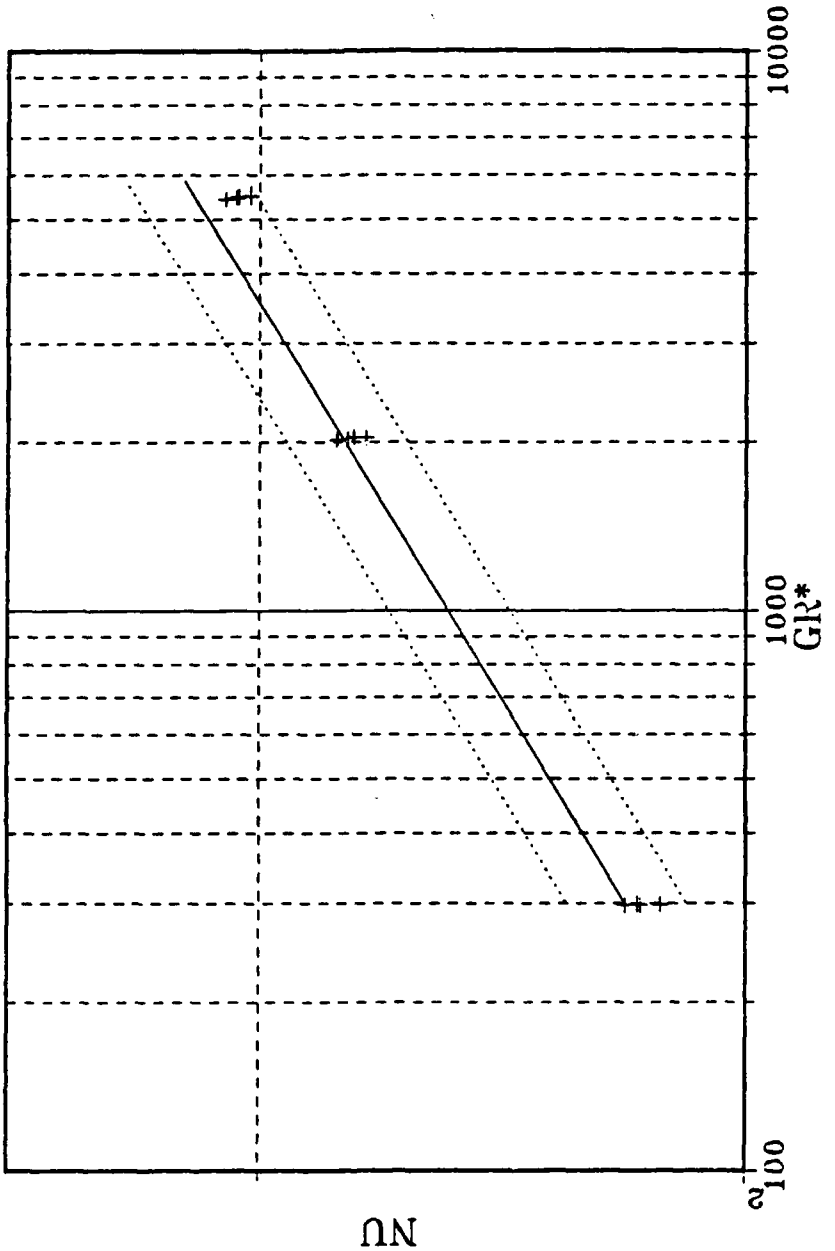

Figure 3.8: Nusselt Number vs. Flux-based Grashof Number with Four Elements Powered

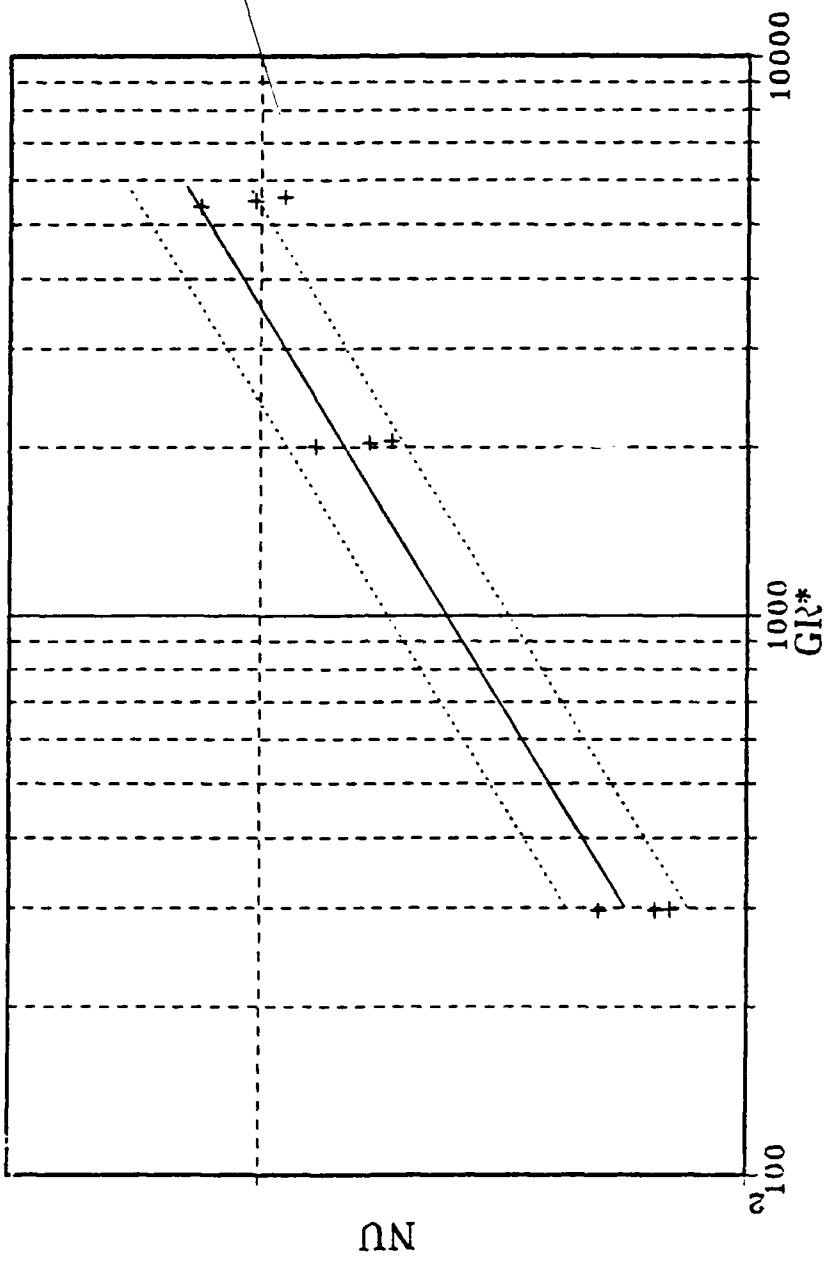

Figure 3.9: Nusselt Number vs. Flux-based Grashof Number with Three Elements Powered

Figure 3.10 suggests that it may be possible to move a shroud wall to within one component height without changing the rate of heat transfer significantly.

The traversing probe was slowly swept spanwise in the z-direction past the centers of the heaters 3, 5 and 8 at a distance of 1.0 mm outward in the y-direction from the heater surface. Resulting temperature variations are shown in Figure 3.11 for a power level of 1.0 watt. The component center is referred to as 0.0. A scale line provides a reference for the width of the heated region of each component. A large drop in temperature is seen to occur beyond $Z = \pm 6$ mm. For the center 50% of each heater, there is relatively small change in temperature, again suggesting a largely two dimensional flow there.

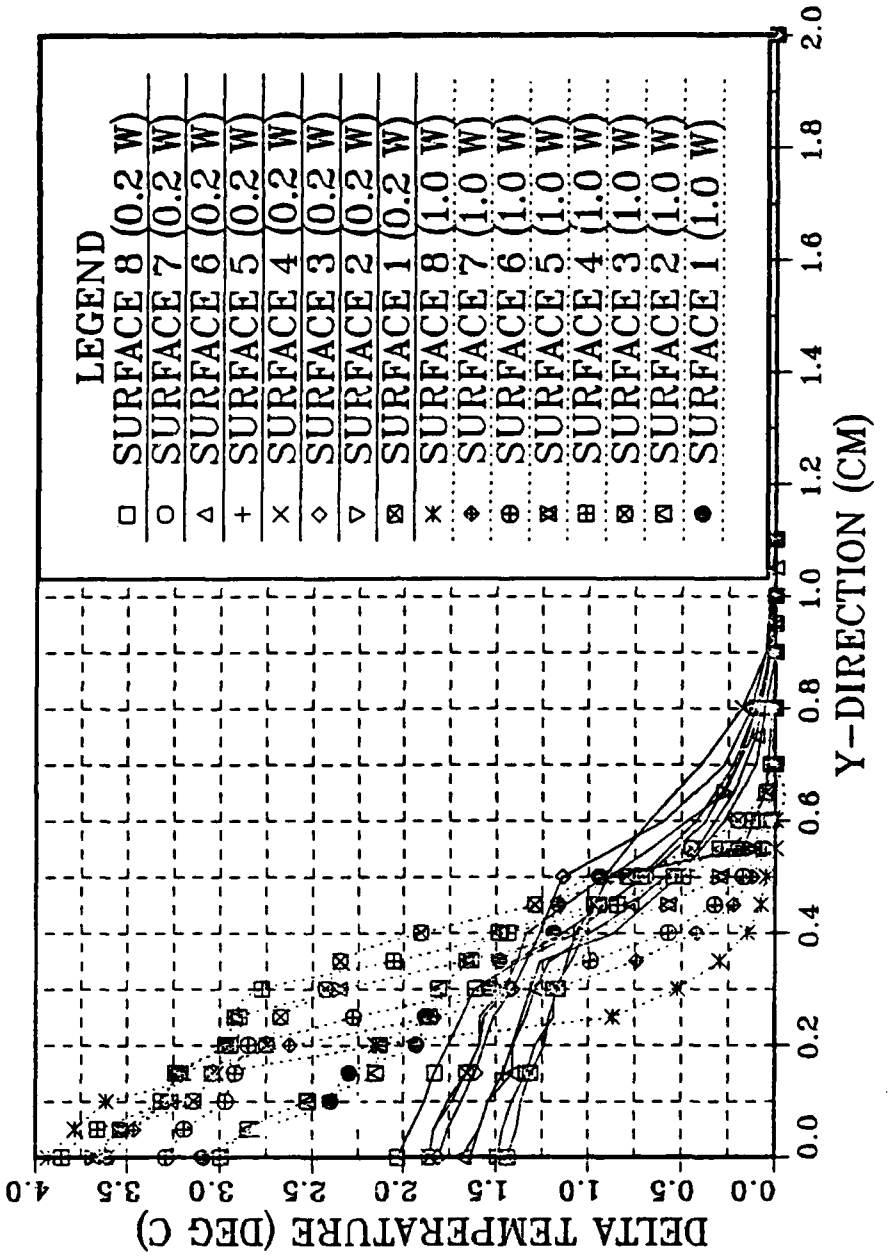

Figure 3.10: Fluid Temperature Distribution in the y-Direction for 0.2 and 1.0 Watts

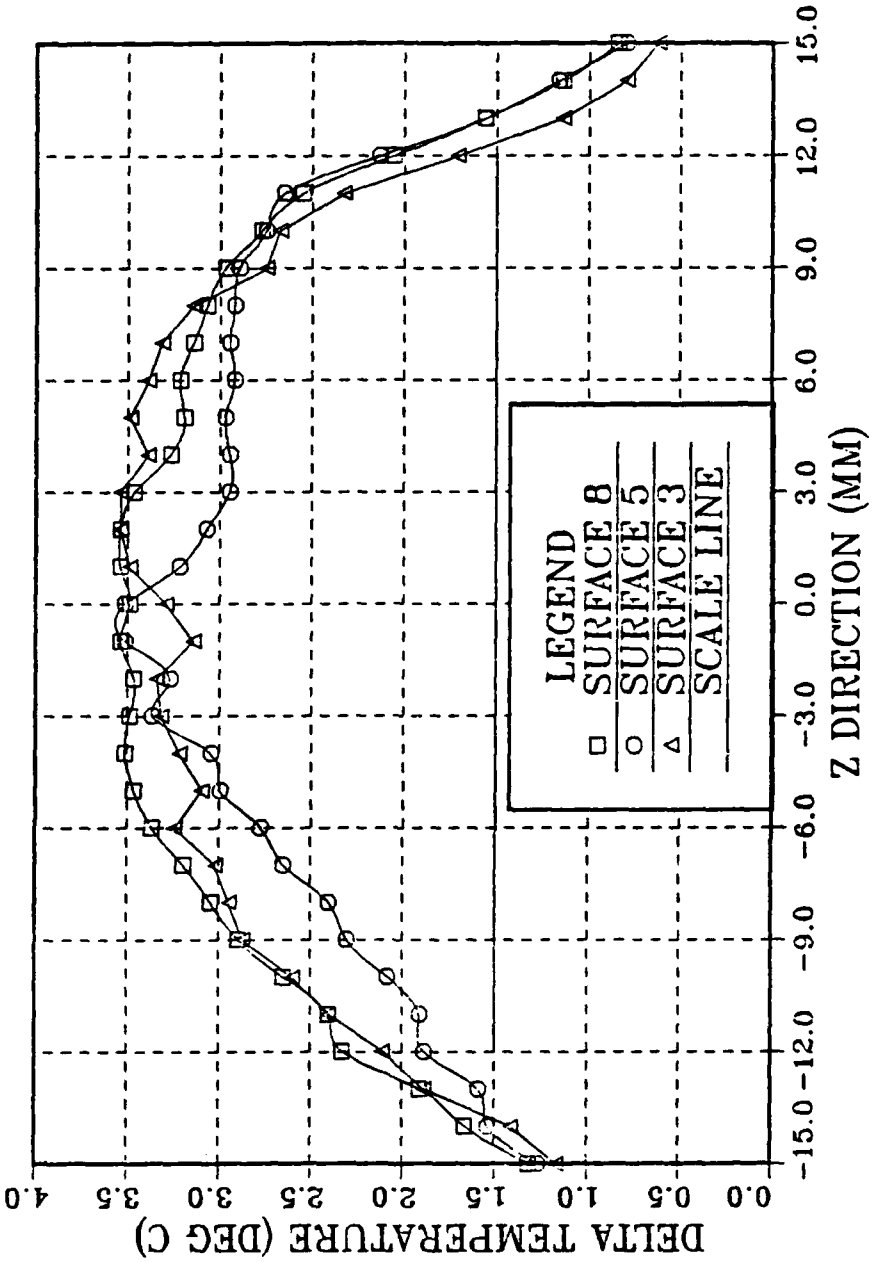

Figure 3.11: Spanwise Fluid Temperature Distribution

IV. TRANSPORT IN A VERTICAL CHANNEL

A plexiglass shroud, simulating the back side of a neighboring circuit board, was positioned to form a vertical channel of various widths.

A. FLOW VISUALIZATION

Useful photographs could only be taken with the shroud positioned no closer than 12 mm from the substrate. All visualizations presented are at power levels of 0.2, 1.0 and 2.0 watts respectively. Figure 4.1 shows the natural convection flow in the x-y plane with the shroud positioned 12 mm from the substrate. The shroud only allows entrainment from the sides and bottom. Initially the flow is not parallel to the channel walls. The entrained fluid entering from the bottom has velocity components in the x and y directions. As the boundary layer develops to the width of the channel, the flow is straightened and conforms to the channel. This same flow behavior occurs when the channel width is increased to 15 mm as shown in Figure 4.2 The effects of entrainment are more noticeable downstream since the boundary layer has more time to develop with the wider channel.

Figure 4.3 presents flow visualization in the x-y plane with the shroud positioned 6 mm from the substrate. These photographs were taken with the camera aligned in the direction normal to the surface. With the shroud in position, side entrainment is much more pronounced than the case without a shroud [Figure 3.2].

B. QUANTITATIVE

Figures 4.4 and 4.5 are non-dimensional representations of temperature excess levels for all center located thermocouples for each shroud condition. These two

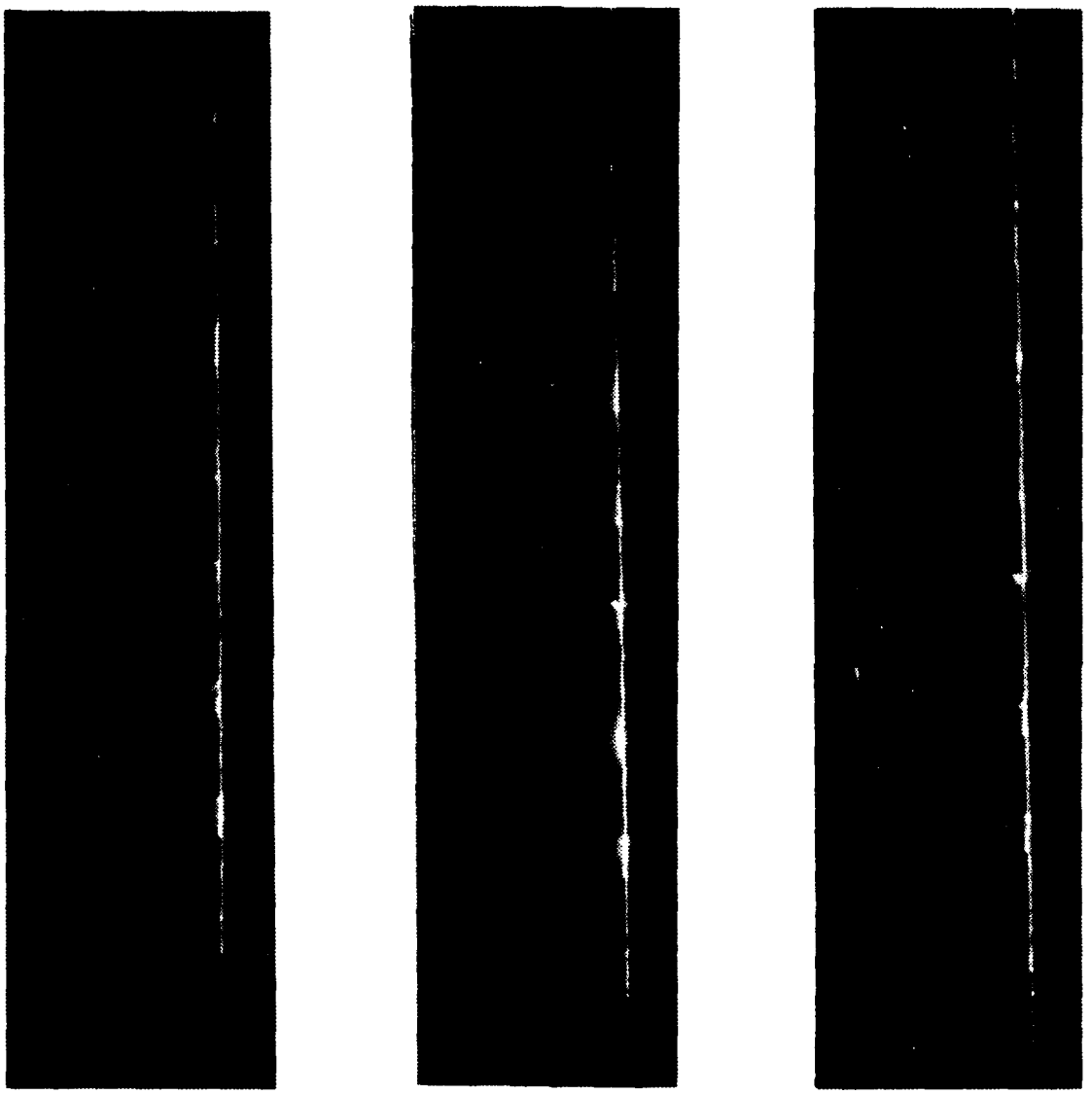

Figure 4.1: Steady Flow in the x-y Plane for Power Levels of 0.2, 1.0 and 2.0 Watts with 12 mm Shroud

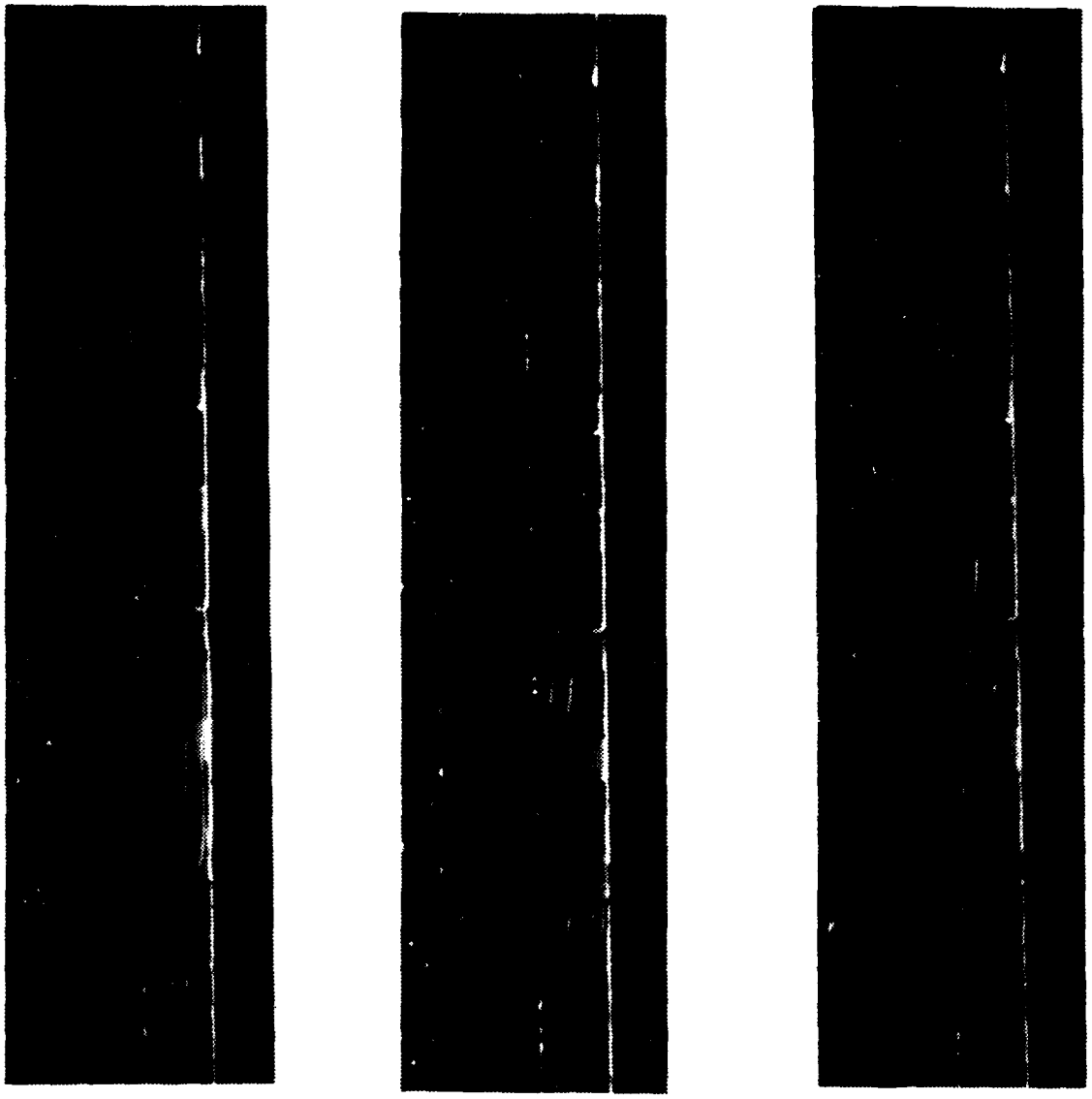

Figure 4.2: Steady Flow in the x-y Plane for Power Levels of 0.2, 1.0, 2.0 Watts with 15 mm Shroud

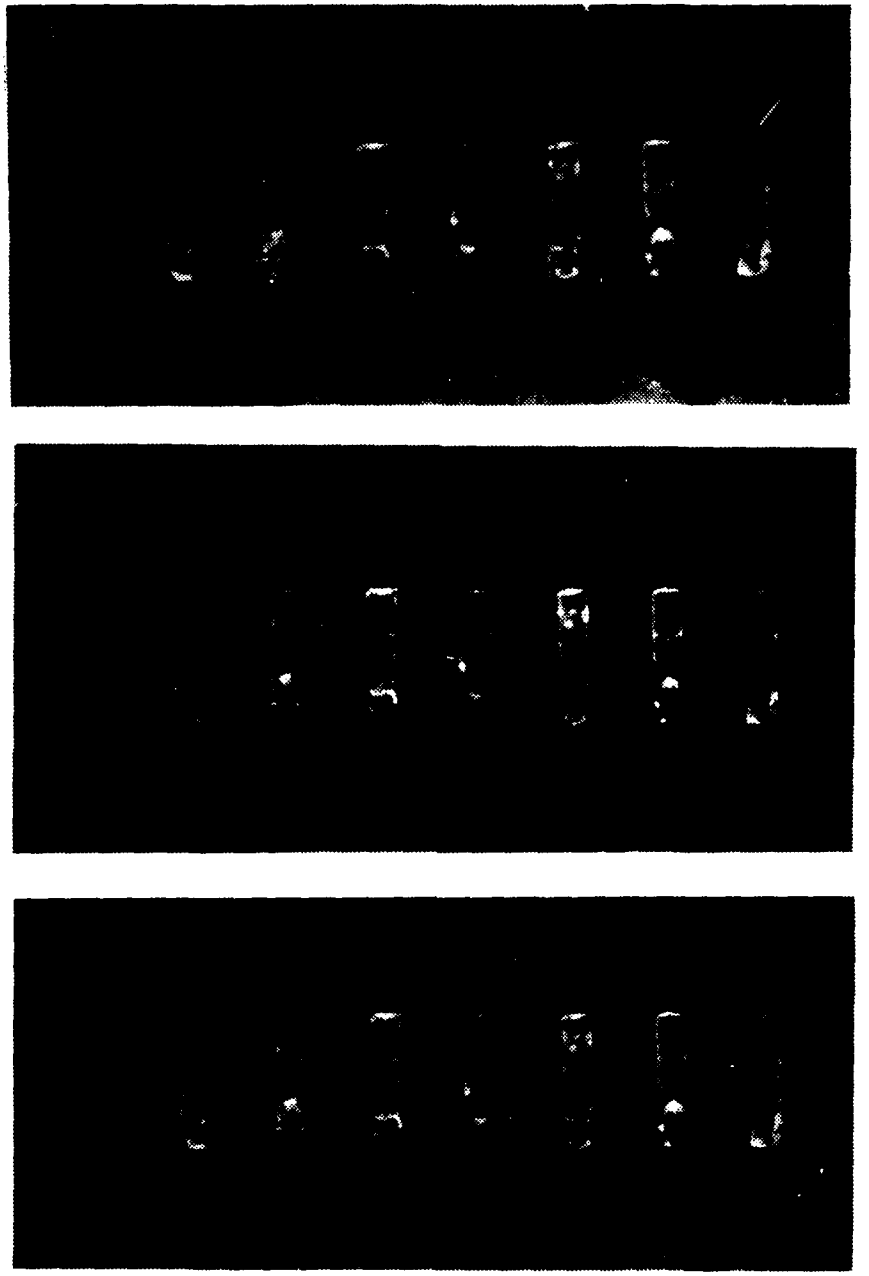

Figure 4.3: Flow in the x-z Plane with 6 mm Shroud Wall

figures depict the spread in data on the same plotting scale for the maximum and minimum power levels.

Again it is noted that the general trend, regardless of input power level, is increasing downstream temperature excess. As power is increased from 0.2 watts to 2.0 watts, the values for the non-dimensional temperature excess decrease. As expected, the heat transfer coefficient increases for corresponding components as the power level increases.

There is little difference in the non-dimensional temperature excess as the shroud is positioned 6 mm or more from the substrate. When the shroud is closer to the substrate, it reduces the ambient fluid entrainment, thereby increasing component temperatures. This is less pronounced at the higher power levels as seen in Figure 4.5.

Figure 4.6 shows the actual temperature difference for the component centers versus the shroud position at 2.0 watts. For this case and all other power levels, the actual temperature difference was greater when the shroud was closer than 6 mm from the substrate. When positioned 6 mm or more from the test surface, the actual temperature difference was within $0.5°C$ of the unshrouded levels.

The modified Nusselt numbers for component centers were calculated using the same correlation as in the previous chapter. These values were compared on a logarithmic plot with the flux-based Grashof numbers at each shroud position. The base line curve for the linear least squares fit of the unshrouded data with $\pm 5\%$ scatterband was also plotted for comparison. The scatter plot for data when the shroud was positioned 1.5 mm from the substrate is shown in Figure 4.7.

The only points in close agreement with base line data are those points corresponding to the leading heater element. Regardless of power level or shroud position, the leading heater can be treated as a single discrete heat source independent

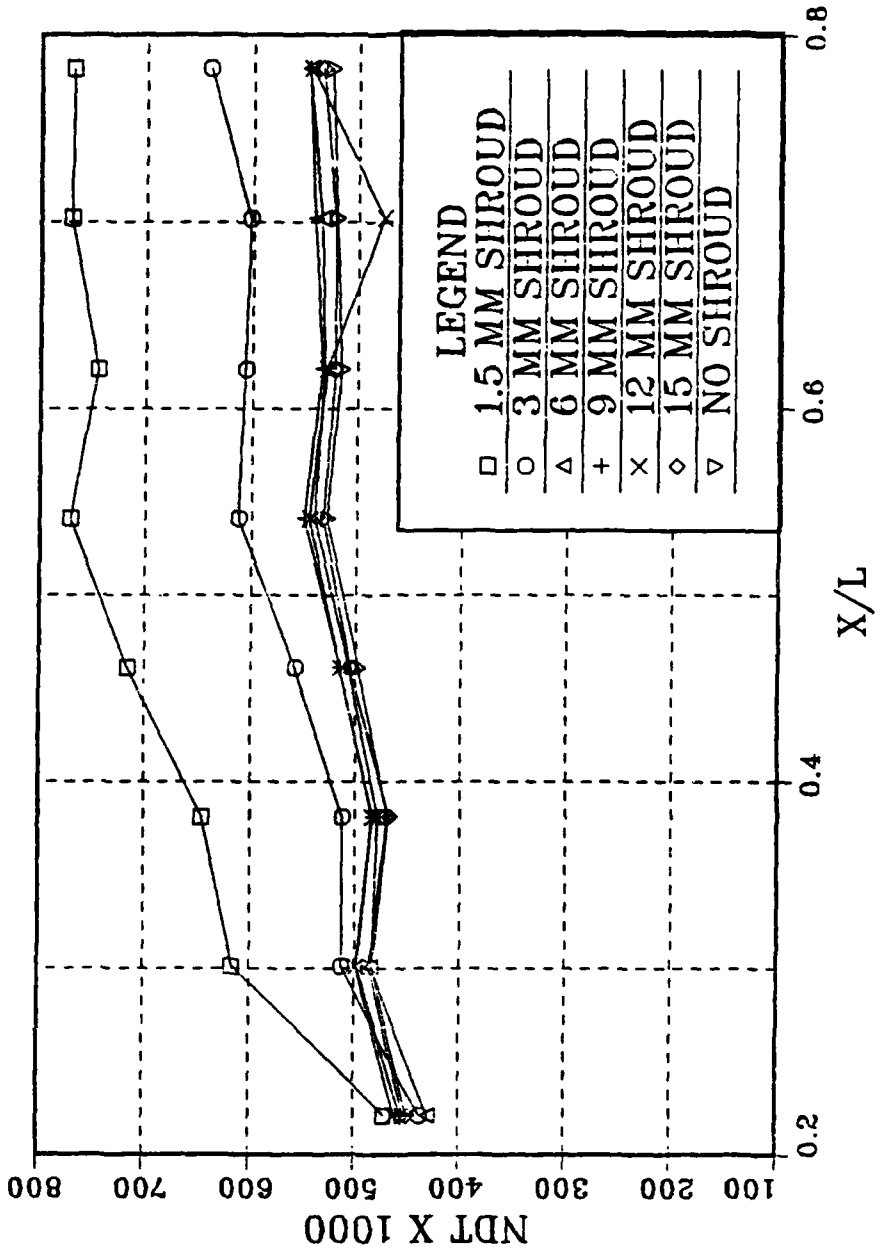

Figure 4.4: Non-dimensional Temperature Excess vs. Position with Shroud at 0.2 Watts

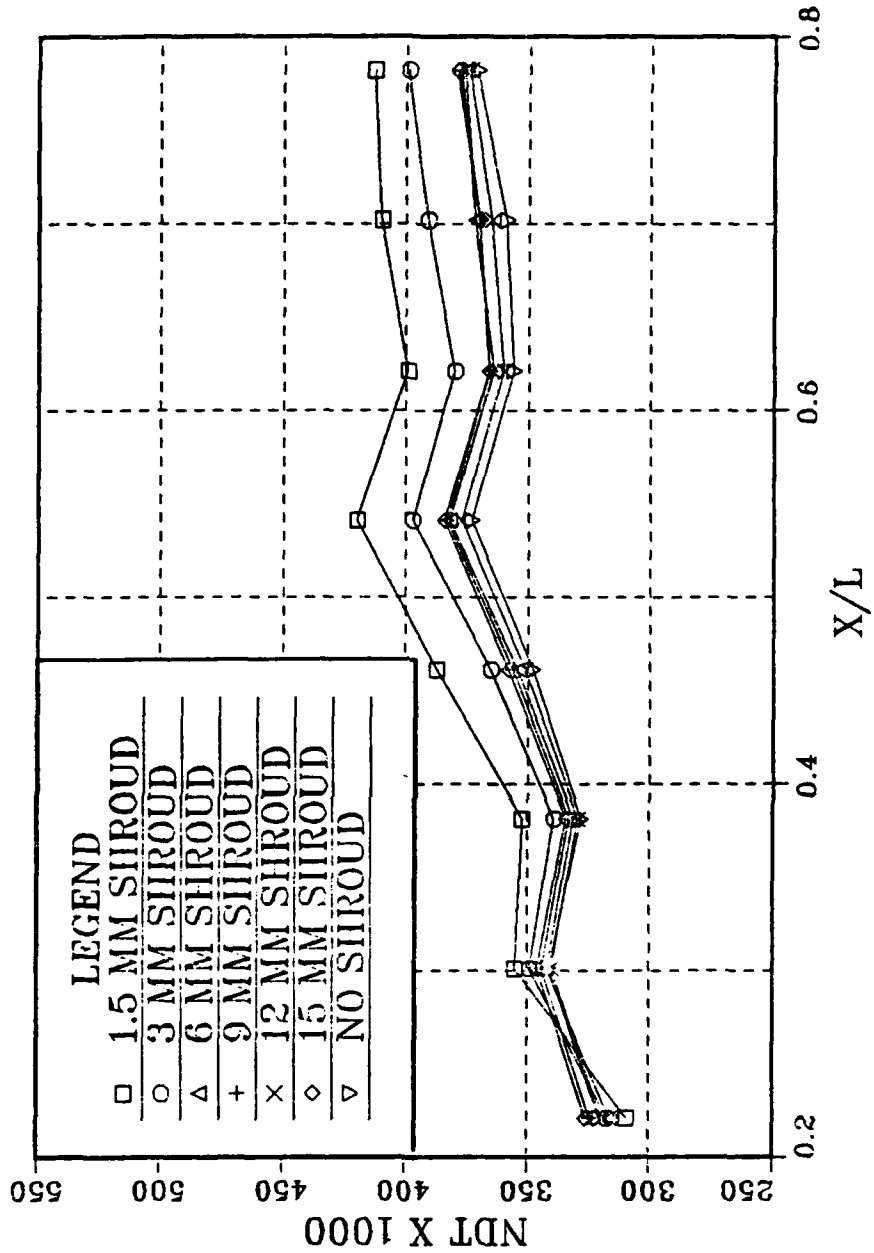

Figure 4.5: Non-dimensional Temperature Excess vs. Position with Shroud at 2.0 Watts

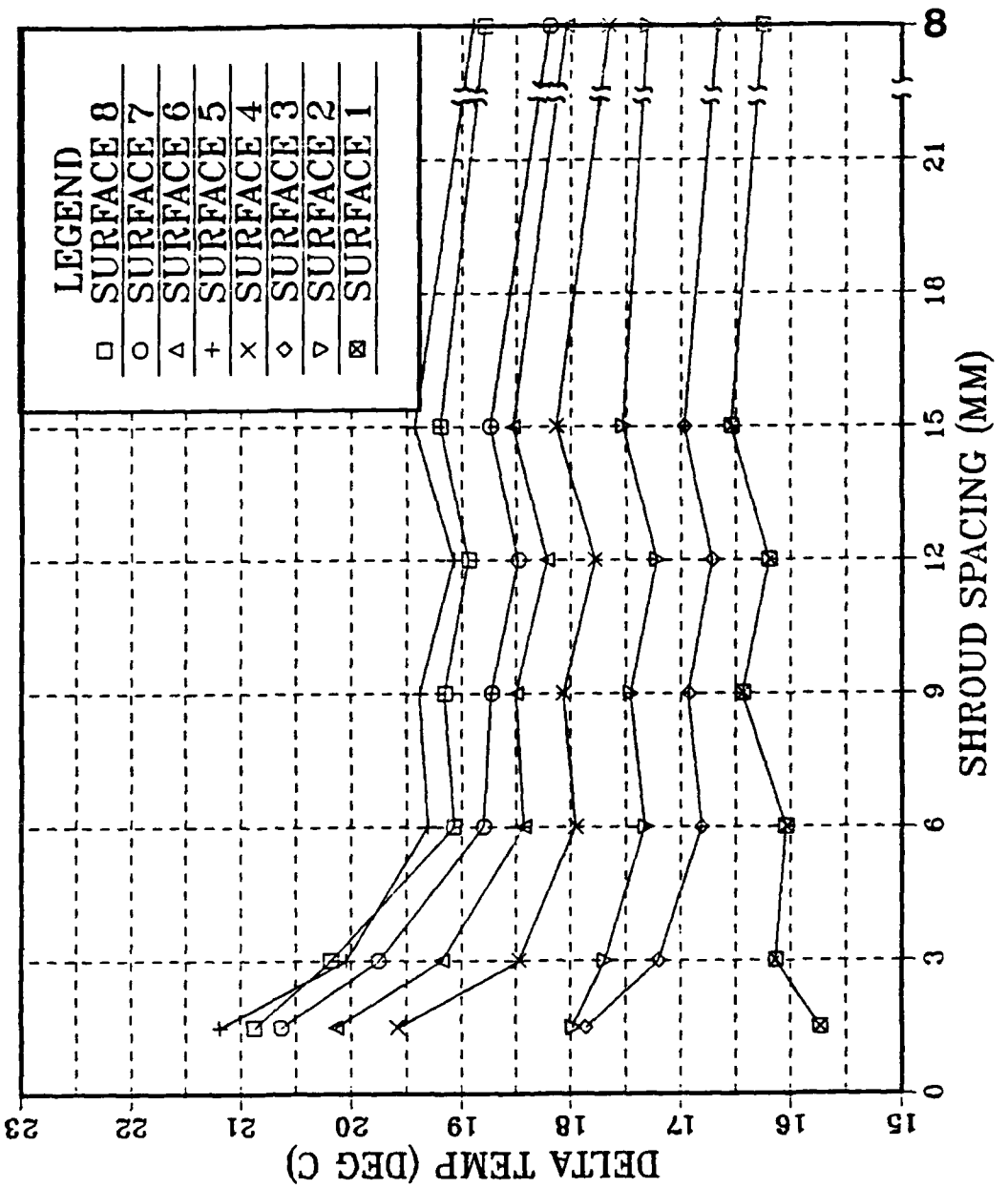

Figure 4.6: Temperature Difference vs. Shroud Spacing: 2.0 Watts

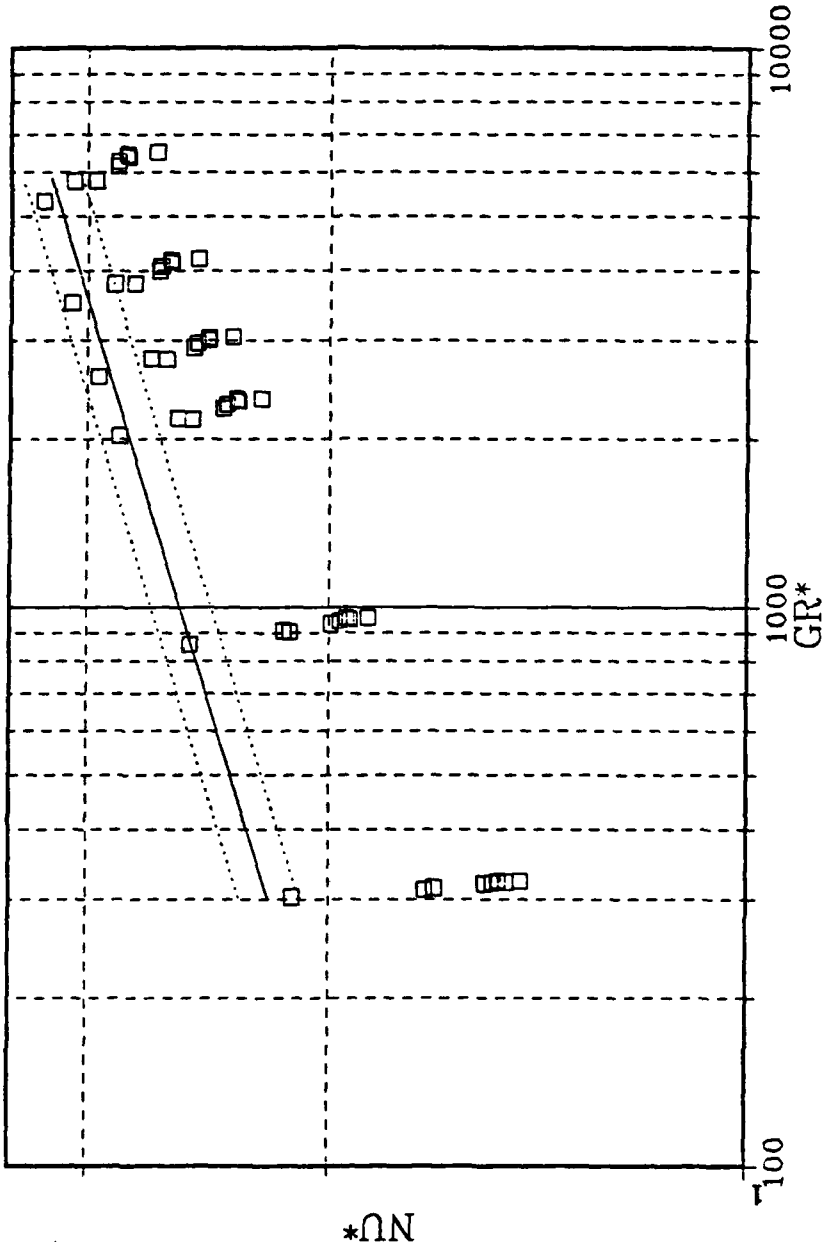

Figure 4.7: Modified Nusselt Number vs. Flux-based Grashof Number with Shroud at 1.5 mm

of downstream array geometry. A scatter plot of data for the shroud position of 3.0 mm is not much better than the previous case.

Figure 4.8 shows a plot of modified data when the shroud spacing is increased to 6.0 mm. The same trends seen here were found at all larger spacings. All data are seen to be in close agreement with the correlating equation thus, with a channel width of 6.0 mm or more in width and for the given geometric array, the modified Nusselt number can be calculated to within 5% accuracy using Equation 3.2 for $250 < Gr_x^* < 7000$ and $Pr \sim 7$.

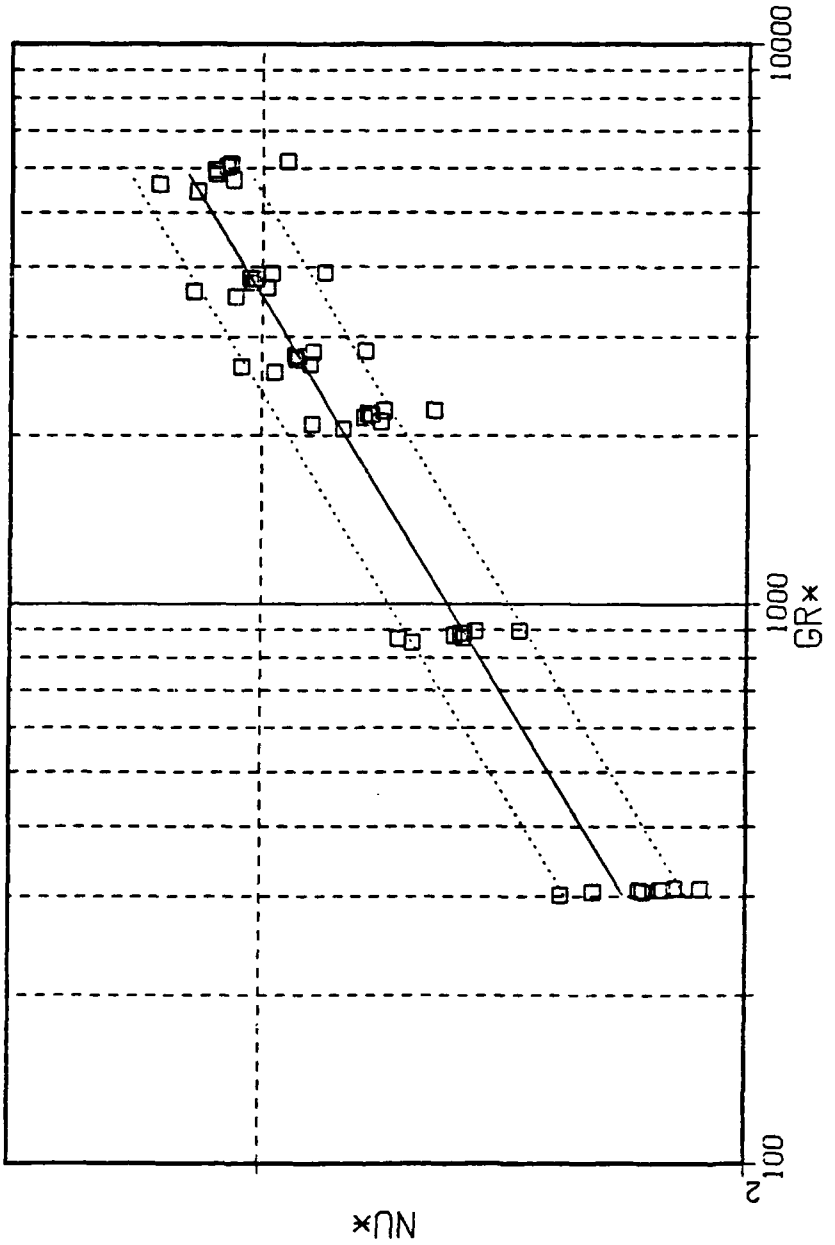

Figure 4.8: Modified Nusselt Number vs. Flux-based Grashof Number with Shroud at 6.0 mm

V. CONCLUSIONS

Flow visualization and quantitative analysis provided several significant conclusions:

- The flow was laminar over the given range of power levels.
- The convective flow is nearly two-dimensional when the shroud is not present. This condition greatly simplifies computational modelling of such flows.
- A thermal layer was embedded within the momentum region. This layer became thinner at increasing levels of heat flux.
- A general trend of increasing component temperatures downstream at each power level was found.
- No significant gain in the rate of heat transfer for channel widths of 6.0 mm or more was found over the unshrouded configuration.
- For geometrically similar arrays, heat transfer relationships for downstream components can be determined by using the correlating equation for this geometry.
- As component spacing is increased to two times or more of that for the present configuration, upstream effects become negligible and the heaters can be treated as an individual discrete heat source.

VI. RECOMMENDATIONS

In continuation of this study, it is suggested to use a similar array, however:

- Study the effects of even smaller component spacings on heat transfer.
- Flank each side of the single array with a column of flush mounted heat sources.
- Spray the heater elements with temperature sensitive liquid crystals.
- Measure the variation of temperature within the thermal layer at higher power levels for all components and spaces between components.
- Explore the transient evolution of transport.

APPENDIX A
SOFTWARE

A. TEMPERATURE ACQUISITION PROGRAM

```
10    !!!!!!!!!!!!!!!!!!!!!!!!!!!!!!!!!!!!!!!!!!!!!!!!!!!!!!!!!!!!!!!!!!!!!!!!!!!!!!!!!!!!!!!!
20    !!                       TEMPERATURE ACQUISITION PROGRAM                       !!
30    !!                               (STEADY STATE)                                !!
40    !!!!!!!!!!!!!!!!!!!!!!!!!!!!!!!!!!!!!!!!!!!!!!!!!!!!!!!!!!!!!!!!!!!!!!!!!!!!!!!!!!!!!!!!
50    REAL Volts(60)
60    REAL Temp(59)
70    CREATE BDAT "_______:,700,0,_",48
80    ASSIGN @Path3 TO "_______:,700,0,_"
90    PRINT "                             SURFACE #8"
100   PRINT
110   OUTPUT 709;"CONFMEAS DCV,100,USE 0"
120   ENTER 709;Volts(60)
130   OUTPUT 709;"CONFMEAS DCV,100-105,USE 0"
140   FOR I=0 TO 5
150   ENTER 709;Volts(I)
160   Temp(I)=.0006797+(25825.1328*Volts(I))-(607789.2467*(Volts(I)*Volts(I)))-(
21952034.3364*(Volts(I)^3))+(8370810996.1874*(Volts(I)^4))+.075
170   PRINT "T. C.  #";I+1,"  Volts D.C.   ";Volts(I),"Temp. DEG. C ";Temp(I)
180   NEXT I
190   PRINT
200   PRINT "                             SURFACE #7"
210   PRINT
220   OUTPUT 709;"CONFMEAS DCV,106-111,USE 0"
230   FOR I=6 TO 11
240   ENTER 709;Volts(I)
250   Temp(I)=.0006797+(25825.1328*Volts(I))-(607789.2467*(Volts(I)*Volts(I)))-(
21952034.3364*(Volts(I)^3))+(8370810996.1874*(Volts(I)^4))+.075
260   PRINT "T. C.  #";I+1,"  Volts D.C.   ";Volts(I),"Temp. DEG. C ";Temp(I)
270   NEXT I
280   PRINT
290   PRINT "                             SURFACE #6"
300   PRINT
310   OUTPUT 709;"CONFMEAS DCV,112-117,USE 0"
320   FOR I=12 TO 17
330   ENTER 709;Volts(I)
340   Temp(I)=.0006797+(25825.1328*Volts(I))-(607789.2467*(Volts(I)*Volts(I)))-(
21952034.3364*(Volts(I)^3))+(8370810996.1874*(Volts(I)^4))+.075
350   PRINT "T. C.  #";I+1,"  Volts D.C.   ";Volts(I),"Temp. DEG. C ";Temp(I)
360   NEXT I
```

```
370   PRINT
380   PRINT "                              SURFACE #3
390   PRINT
400   OUTPUT 709;"CONFMEAS DCV,180-189,USE 0"
410   FOR I=10 TO 19
420   ENTER 709;Volts(I)
430   Temp(I)=.0006797+(25825.1328*Volts(I))-(607789.2467*(Volts(I)*Volts(I)))+(
21952034.3364*(Volts(I)^3))+(8370810996.1874*(Volts(I)^4))+.075
440   PRINT "T. C.  #";I+1,"  Volts D.C.  ";Volts(I),"Temp. DEG. C ";Temp(I)
450   NEXT I
460   OUTPUT 709;"CONFMEAS DCV,200-203,USE 0"
470   FOR I=20 TO 23
480   ENTER 709;Volts(I)
490   Temp(I)=.0006797+(25825.1328*Volts(I))-(607789.2467*(Volts(I)*Volts(I)))+
21952034.3364*(Volts(I)^3)+(8370810996.1874*(Volts(I)^4))+.075
500   PRINT "T. C.  #";I-1,"  Volts D.C.  ";Volts(I),"Temp. DEG. C ";Temp(I)
510   NEXT I
520   PRINT
530   PRINT "                              SURFACE #4"
540   PRINT
550   OUTPUT 709;"CONFMEAS DCV,204-209,USE 0"
560   FOR I=24 TO 29
570   ENTER 709;Volts(I)
580   Temp(I)=.0006797+(25825.1328*Volts(I))-(607789.2467*(Volts(I)*Volts(I)))+(
21952034.3364*(Volts(I)^3))+(8370810996.1874*(Volts(I)^4))+.075
590   PRINT "T. C.  #";I+1,"  Volts D.C.  ";Volts(I),"Temp. DEG. C ";Temp(I)
600   NEXT I
610   PRINT
620   PRINT "                              SURFACE #5"
630   PRINT
640   OUTPUT 709;"CONFMEAS DCV,210-215,USE 0"
650   FOR I=30 TO 35
660   ENTER 709;Volts(I)
670   Temp(I)=.0006797+(25825.1328*Volts(I))-(607789.2467*(Volts(I)*Volts(I)))+(
21952034.3364*(Volts(I)^3))+(8370810996.1874*(Volts(I)^4))+.075
680   PRINT "T. C.  #";I+1,"  Volts D.C.  ";Volts(I),"Temp. DEG. C ";Temp(I)
690   NEXT I
700   FOR J=1 TO 14
710   PRINT
```

```
720   NEXT J
730   PRINT "                              SURFACE #2"
740   PRINT
750   OUTPUT 709;"CONFMEAS DCV,216-219,USE 0"
760   FOR I=36 TO 39
770   ENTER 709;Volts(I)
780   Temp(I)=.0006797+(25825.1328*Volts(I))-(607789.2467*(Volts(I)*Volts(I)))-(
21952034.3364*(Volts(I)^3))+(8370810996.1874*(Volts(I)^4))+.075
790   PRINT "T. C.  #";I+1,"  Volts D.C.  ";Volts(I),"Temp. DEG. C ";Temp(I)
800   NEXT I
810   OUTPUT 709;"CONFMEAS DCV,300-301,USE 0"
820   FOR I=40 TO 41
830   ENTER 709;Volts(I)
840   Temp(I)=.0006797+(25825.1328*Volts(I))-(607789.2467*(Volts(I)*Volts(I)))-(
21952034.3364*(Volts(I)^3))+(8370810996.1874*(Volts(I)^4))+.075
850   PRINT "T. C.  #";I+1,"  Volts D.C.  ";Volts(I),"Temp. DEG. C ";Temp(I)
860   NEXT I
870   PRINT
880   PRINT "                              SURFACE #1"
890   PRINT
900   OUTPUT 709;"CONFMEAS DCV,302-307,USE 0"
910   FOR I=42 TO 47
920   ENTER 709;Volts(I)
930   Temp(I)=.0006797+(25825.1328*Volts(I))-(607789.2467*(Volts(I)*Volts(I)))-(
21952034.3364*(Volts(I)^3))+(8370810996.1874*(Volts(I)^4))+.075
940   PRINT "T. C.  #";I+1,"  Volts D.C.  ";Volts(I),"Temp. DEG. C ";Temp(I)
950   NEXT I
960   !OUTPUT @Path3;Temp(*)
970   PRINT
980   PRINT
990   PRINT "               BATH TEMPERATURES (TOP TO BOTTOM)"
1000  PRINT
1010  OUTPUT 709;"CONFMEAS DCV,317-319,USE 0"
1020  FOR I=57 TO 59
1030  ENTER 709;Volts(I)
1040  Temp(I)=.0006797+(25825.1328*Volts(I))-(607789.2467*(Volts(I)*Volts(I)))-(
21952034.3364*(Volts(I)^3))+(8370810996.1874*(Volts(I)^4))+.075
1050  PRINT "VOLTS D.C.  ";Volts(I),"TEMP. DEG. C ";Temp(I)
1060  NEXT I
1070  END
```

B. DATA REDUCTION PROGRAM

```
10    !!!!!!!!!!!!!!!!!!!!!!!!!!!!!!!!!!!!!!!!!!!!!!!!!!!!!!!!!!!!!!!!!!!!!!
20    !!                                                                  !!
30    !!                     DATA REDUCING PROGRAM                        !!
40    !!                                                                  !!
50    !!!!!!!!!!!!!!!!!!!!!!!!!!!!!!!!!!!!!!!!!!!!!!!!!!!!!!!!!!!!!!!!!!!!!!
60    REAL T(48),Qcond(8)
70    REAL Power,Tamb,G,Kpg,Delx,As,Per,Ta,Qconv,Lbar
80    REAL Qflux,Delt,Tfilm,Beta,Spvol,Dynvisc
90    REAL Kinvisc,Kf,Pr,Theta,Ndt,Hx,Grmod,Hux,Lnu,Lgr
100   PRINTER IS 1
110   PRINT "INPUT DATA FILE NAME"
120   INPUT Filename$
130   PRINT
140   PRINT "INPUT POWER VALUE IN WATTS"
150   INPUT Power
160   PRINT
170   PRINT "INPUT SHROUD SPACING IN mm"
180   INPUT Space$
190   PRINT
200   PRINT "INPUT AMBIENT TEMPERATURE"
210   INPUT Tamb
220   PRINTER IS 701
230   PRINT "POWER LEVEL (WATTS)      :",Power
240   PRINT
250   PRINT "SHROUD POSITION (mm)     :",Space$
260   PRINT
270   PRINT "AMBIENT TEMPERATURE (C) :",Tamb
280   PRINT
290   PRINT
300   ASSIGN @Path TO Filename$
310   ENTER @Path;T(*)
320   G=9.81
330   Kpg=.1421
340   Delx=.006731
350   As=.0239*.0078
360   Per=2*.0239+2*.0078
370   Lbar=As/Per
380   A$="Qcond"
```

```
390   B$="X/L"
400   C$="NDT"
410   D$="LOG(Nux)"
420   E$="LOG(Grx*)"
430   F$="DELT"
440   G$="Hx"
450   H$="Nux"
460   I$="Grx*"
470   !!!!!!!!!!!!!!!!!!!!!!!!!!!!!!!!!!!!!!!!!!!!!!!!!!!
480   !              COMPUTE CONDUCTION LOSSES                !
490   !!!!!!!!!!!!!!!!!!!!!!!!!!!!!!!!!!!!!!!!!!!!!!!!!!!
500   J=8
510   FOR I=0 TO 42 STEP 6
520   Ta=(T(I)+T(I+1)+T(I+2)+T(I+3)+T(I+4))/5
530   Qcond(J)=As*Kpg*(Ta-T(I+5))/Delx
540   J=J-1
550   NEXT I
560   !!!!!!!!!!!!!!!!!!!!!!!!!!!!!!!!!!!!!!!!!!!!!!!!!!!
570   N=0
580   FOR J=8 TO 1 STEP -1
590   Cnt=0
600   Xt=((J-1)*25.4+74)/317
610   Xb=((J-1)*25.4+66)/317
620   Xc=((J-1)*25.4+70)/317
630   PRINT
640   PRINT
650   PRINT "                                       SURFACE #",J
660   PRINT
670   PRINT USING "2X,AAAAA,4X,AAA,4X,AAA,4X,AAAAAAAA,2X,AAAAAAAAA,3X,AAAA,5X,AA
,6X,AAA,4X,AAAA";A$,B$,C$,D$,E$,F$,G$,H$,I$
680   FOR I=N TO N+4
690   Qconv=Power-Qcond(J)
700   Qflux=Qconv/As
710   Delt=T(I)-Tamb
720   Tfilm=273.15+(T(I)+Tamb)/2
730   Beta=(-7.944856E-8*(Tfilm^2))+(5.7356479E-5*Tfilm)-.0097810563
740   Spvol=(4.69699E-9*(Tfilm^2))+(-2.53745E-6*Tfilm)+.001341903
750   Dynvisc=(3.2348511E-7*(Tfilm^2))+(-.00021474487*Tfilm)+.036166792
760   Kinvisc=Spvol*Dynvisc
```

```
770   Kf=(1.418181818E-3*Tfilm)+.1866
780   Pr=(4.65706E-3*(Tfilm^2))+(-2.922094*Tfilm)+463.3319
790   Theta=Qflux*Lbar/Kf
800   Ndt=Delt/Theta
810   Hx=Qflux/Delt
820   Grmod=(G*Beta*Qflux*(Lbar)^4)/(Kf*Kinvisc^2)
830   Nux=Hx*Lbar/Kf
840   Lgr=LGT(Grmod)
850   Lnu=LGT(Nux)
860   IF Cnt=0 THEN Xtol=Xt
870   IF Cnt=1 THEN Xtol=Xb
880   IF Cnt>1 THEN Xtol=Xc
890   Cnt=Cnt+1
900   PRINT USING "1X,D.DDDD,2X,D.DDD,2X,D.DDD,4X,D.DDD,7X,D.DDD,4X,DD.DDD,2X,DD
DD.D,2X,DD.DDD,2X,DDDD.D";Qcond(J),Xtol,Ndt,Lnu,Lgr,Delt,Hx,Nux,Grmod
910   NEXT I
920   N=N+8
930   NEXT J
940   END
```

APPENDIX B
EQUATIONS

A. SAMPLE CALCULATIONS

These calculations are based on temperatures from data corresponding to surface eight with all elements powered to 1.0 Watt and no shroud.

1. CHARACTERISTIC DIMENSIONS

$$\begin{aligned} P &= 2(0.0078 + 0.0239) \\ &= 0.063m \end{aligned} \tag{B.1}$$

$$\begin{aligned} A_s &= (0.0078)(0.0239) \\ &= 1.864 \times 10^{-4} m^2 \end{aligned} \tag{B.2}$$

$$\begin{aligned} \bar{L} &= \frac{1.864 \times 10^{-4}}{0.0634} \\ &= 2.940 \times 10^{-3} m \end{aligned} \tag{B.3}$$

2. CONDUCTION LOSS

$$\begin{aligned} T_{avg} &= \frac{30.40 + 27.98 + 27.09 + 27.39 + 31.11}{5} \\ &= 28.79°C \end{aligned} \tag{B.4}$$

$$\begin{aligned} Q_{COND} &= \frac{(1.864 \times 10^{-4})(0.1421)(28.79 - 26.09)}{.006731} \\ &= 0.0106W \end{aligned} \tag{B.5}$$

3. CONVECTED HEAT FLUX

$$Q_{CONV} = 1.0 - 0.0106$$

$$= 0.9894W \tag{B.6}$$

$$q'' = \frac{0.9894}{1.864 \times 10^{-4}}$$

$$= 5308\frac{W}{m^2} \tag{B.7}$$

4. FLUID PROPERTIES

$$T_{film} = \frac{31.11 + 20.55}{2} + 273.15$$

$$= 298.98K \tag{B.8}$$

$$\beta = (-7.945 \times 10^{-8})(298.98) + (5.736 \times 10^{-5})$$

$$(298.98) - 9.781 \times 10^{-3}$$

$$= 2.665 \times 10^{-4}K^{-1} \tag{B.9}$$

$$v = (4.697 \times 10^{-9})(298.98)^2 - (2.537 \times 10^{-6})(298.98)$$

$$+1.342 \times 10^{-3}$$

$$= 1.003 \times 10^{-3}\frac{m^3}{kg} \tag{B.10}$$

$$\mu = (3.235 \times 10^{-7})(298.98)^2 - (2.147 \times 10^{-4})(298.98)$$

$$+0.0362$$

$$= 9.264 \times 10^{-4}\frac{Ns}{m^2} \tag{B.11}$$

$$\nu = (1.003 \times 10^{-3})(9.264 \times 10^{-4})$$

$$= 9.262 \times 10^{-7}\frac{m^2}{s} \tag{B.12}$$

$$k_f = (1.418 \times 10^{-3})(298.98) + 0.1866$$

$$= 0.611\frac{W}{mK} \tag{B.13}$$

5. NON-DIMENSIONAL TEMPERATURE EXCESS

$$\theta = 31.11 - 20.55 = 10.56°C \tag{B.14}$$

$$\theta_o = \frac{(5308)(2.940 \times 10^{-3})}{0.611} = 25.54°C \quad \text{(B.15)}$$

$$NDT = \frac{10.56}{25.54} = 0.413 \quad \text{(B.16)}$$

6. HEAT TRANSFER COEFFICIENT

$$h_x = \frac{5308}{31.11 - 20.55} = 502.7 \frac{W}{m^2 K} \quad \text{(B.17)}$$

7. FLUX-BASED GRASHOF NUMBER

$$Gr_x^* = \frac{(9.81)(2.665 \times 10^{-4})(5308)(2.940 \times 10^{-3})^4}{(0.611)(9.292 \times 10^{-7})^2} = 1965 \quad \text{(B.18)}$$

8. NUSSELT NUMBER

$$Nu = \frac{(502.7)(2.940 \times 10^{-3})}{0.611} = 2.419 \quad \text{(B.19)}$$

LIST OF REFERENCES

1. Hannemann, R., Incropera, F. P., and Simons, R., "Single Phase Liquid Cooling," *Research Needs in Electronic Cooling*, pp. 6-25, December 1986.
2. Milanez, L. F. and Bergles, A. E., "Studies on Natural Convection Heat Transfer from Thermal Sources on a Vertical Surface," *Proceedings of the Eighth International Heat Transfer Conference*, Vol. 3, pp. 1347-1352, 1986.
3. Johnson, C. B., "Evaluation of Correlations for Natural Convection Cooling of Electronic Equipment," *Heat Transfer Engineering*, Vol. 7, pp. 36-45, 1986.
4. Park, K. A. and Bergles, A. E., "Natural Convection Heat Transfer Characteristics of Simulated Microelectronic Chips," *Journal of Heat Transfer - 1987*, ASME, HTD-Vol. 109, pp.90-96.
5. Hazard, S. J., "Single Phase Liquid Immersion Cooling of Discrete Heat Sources in a Vertical Channel," M.S.M.E. Thesis, Naval Postgraduate School, Monterey,CA , December 1987.
6. Baker, E., "Liquid Cooling of Microelectronic Devices by Free and Forced Convection," *Microelectronics and Reliability*, Pergamon Press, Vol. 11, pp. 213-222, 1972.
7. Willson, T. D., "A Study of Natural Convection Cooling of Multiple Discrete Heat Sources in a Vertical Channel," M.S.M.E. Thesis, Naval Postgraduate School, Monterey, CA , June 1988.
8. Incropera, F. P., and DeWitt, D. P., *Fundamentals of Heat and Mass Transfer*, p. 774, John Wiley and Sons, 1981.

INITIAL DISTRIBUTION LIST

		No. of Copies
1.	Defense Technical Information Center Cameron Station Alexandria, VA 22304-6145	2
2.	Library, Code 0142 Naval Postgraduate School Monterey, CA 93943-5002	2
3.	Mr. Howard Stevens Head, Electrical Research Center David Taylor Research Center Annapolis, MD 21402	1
4.	Superintendent Naval Postgraduate School Attn: Professor A. J. Healey, Code 69Hy Department of Mechanical Engineering Monterey, CA 93943-5004	1
5.	Superintendent Naval Postgraduate School Attn: Professor Y. Joshi, Code 69Ji Department of Mechanical Engineering Monterey, CA 93943-5004	3
6.	Superintendent Naval Postgraduate School Attn: Professor M. D. Kelleher, Code 69Kk Department of Mechanical Engineering Monterey, CA 93943-5004	1
7.	Superintendent Naval Postgraduate School Attn: Professor A. D. Kraus, Code 62Ks Department of Electrical and Computer Engineering Monterey, CA 93943-5004	1

8. Mr. Duane Embree — 1
Naval Weapons Support Center
Code 0642
Crane, IN 47522

9. Superintendent — 1
Naval Postgraduate School
Attn: Curricular Officer, Code 34
Monterey, CA 93943-5004

10. Superintendent — 1
Naval Postgraduate School
Attn: Lt. Al Gaiser
SMC 2007
Monterey, CA 93943-5000

11. Mr. Joseph Cipriano — 1
Executive Director
Weapons and Combat Systems Directorate
Naval Sea Systems Command
Washington, D.C. 20362-5101

12. Lt. Daniel L. Knight — 1
Rt. 1, Box 224A
Warrenville, S.C. 29851